Hydrodynamics affecting larval transport and settlement onto intertidal oyster reefs

Elizabeth Rose Whitman

Bachelor of Arts, Purdue University, 2006

A Thesis presented to the Graduate Faculty

of the University of Virginia in Candidacy for the Degree of

Master of Science

Department of Environmental Sciences

University of Virginia

March, 2011

Matthew A. Reidenbach

M. G. McCormick-Ray

K. M. Kibler

Carl Hershner

Abstract

The Eastern Oyster (*Crassostrea virginica*) once played a pivotal ecological role in Virginia waters and the Chesapeake Bay. However, unregulated over-harvesting, combined with reduced water quality and disease, has caused a drastic decline in oyster populations, such that present day levels are less than 2% of pre-harvest populations. Restoration efforts, currently underway to re-establish healthy oyster populations, are focused on rehabilitating benthic habitat to be suitable for natural oyster larval recruitment and growth. The goal of this study was to understand the hydrodynamics involved in fluid and sediment transport over reefs, and how these dynamics may impact larval transport to healthy and restored reef areas.

Velocity and turbulence data was collected off of the Eastern shore of Virginia over multiple benthic surfaces including a mud flat, a healthy reef, and two restoration sites comprised of either fossil oyster or whelk shell. Reynolds stresses, shear velocity, u_*, and drag coefficients, C_D, were computed and due to the extreme roughness of the reef, mean estimates of u_* over a healthy reef were found to be 47% greater than those found over a restoration site. Enhanced shear increased both turbulent mixing and drag above the reef, but within the interstitial areas between individual oysters, mean velocities and turbulent motions were reduced. C_D, used as a measure of roughness, also increased with elevation on the healthy reef.

Small-scale hydrodynamic forces were studied in an open-channel, recirculating, water flume along benthic roughnesses of varying height and spacing, used to mimic

variability found on the reef. Drag and lift forces within the structure decreased with increasing height and increased with increased spacing. Geometrically similar slate tile structures were deployed in the field over a five month period, and the greatest larval recruitment corresponded closely to locations where drag and lift forces were reduced. The combined field and laboratory data suggests that restoration efforts should consider both elevation and bed roughness similar to those found on healthy oyster reefs, to provide suitable hydrodynamic conditions that promote larval recruitment, prevent burial by sediment, and may provide some refuge from predation.

Table of Contents Page

Chapter 1

Introduction and literature review

1.1 Background

The Eastern Oyster (*Crassostrea virginica*) can be found from as far south as Argentina to as far north as the Gulf of St. Lawrence in Canada where they inhabit estuaries and coastal waters (Carriker and Gaffney 1996). With their historical prevalence and subsequent decades of decline in Virginia waters and Chesapeake Bay, their role in physical-biological coupling (Lenihan, 1999) and in local ecosystem services (Nelson *et al.*, 2004) has come into the spotlight. Fish and many invertebrates use oyster reefs as foraging grounds, so healthy oyster reefs promote estuarine biodiversity (Arve 1960, Bahr and Lanier 1981, Zimmerman *et al.* 1989, Lenihan *et al.* 1998). As well as providing historically important benthic substrate and habitat for other species (McCormick-Ray 1998), oysters are also important to the water quality of the shallow lagoons where the reefs are located. As filter feeders, they filter algae and detritus from the water improving both water quality and water clarity and deposit fecal material to the sea floor, (Newell 1988). There is currently a debate in the literature over the ability of *C. virginica* to control phytoplankton blooms in the Chesapeake Bay (Newell 1988, Pomeroy *et al.* 2006, Newell *et al.* 2007, Pomeroy *et al.* 2007), but their ability to clear water on a smaller scale and modify their local environment is well documented (e.g. Nelson *et al.*, 2004; Porter *et al.*, 2004; Cerco and Noel, 2007).

Despite the importance of oysters to the local ecosystem, over fishing, disease and poor management practices have resulted in the loss of 99% of the historical biomass of *C. virginica* in the Chesapeake Bay (Rothschild *et al.* 1994, Kemp *et al.* 2005). There are now increased efforts to restore and manage oyster reefs (Rothschild *et al.* 1994 Cerco and Noel 2007, Schulte *et al.* 2009), and agencies such as The Nature Conservancy are relying on continued research that could provide insight into the parameters that must be considered to achieve successful restoration. Some of these parameters include disease susceptibility, predation, and environmental conditions.

Dense concentrations of the filter feeders comprise unharvested oyster reefs (Figure 1.1) (Dame *et al.* 1984). Due to reef expansion, both horizontally and vertically as a result of oysters settling and growing on each other, they affect processes such as sedimentation (McCormick-Ray 1998) and particulate organic carbon removal by means of biofiltration as well as physical factors (Dame *et al.* 1984). For reefs to develop, oysters must survive a larval phase as planktotrophic larvae extending several weeks (Loosanoff 1965, Coen *et al.* 2000), attach to substrata, and grow from spat to large individuals. *C. virginica* spawning and growth rates are highest when the water temperature is around 25°C and vary with temperature ranging 6–32°C (Galtsoff 1964), and the majority of reefs are intertidal or found in areas of low salinity (<15 ppt) (Coen *et al.* 2000). Spawning from year to year is significant not only for continuing recruitment but the larvae serve as food for other aquatic animals (Loosanoff 1965). Since water temperature is not controllable on a short time scale, restoration efforts are focused on

creating suitable benthic environments for recruitment in which sanctuaries can protect areas where oysters grow into spawning adults (Brumbaugh *et al.* 2000).

Figure 1.1: Oyster reef found within the Hillcrest reef tract, a TNC sanctuary (see Figure 2.1)

Recent restoration successes have been seen in sanctuary areas of the Chesapeake Bay where studies have found that the higher the vertical relief of the oyster reef, the more successful is the recruitment and growth of oysters (Schulte *et al.* 2009). Overall, a five-fold increase in living oyster densities was found, and attributed to the high relief of the successful oyster reefs. Hydrodynamic conditions over these reefs should be different than the hydrodynamic conditions over the low relief reefs because of factors such as water depth and benthic roughness. Lenihan *et al.* 1996 showed that the growth, condition and survival of oysters are positively correlated to an increase in flow velocity. It is reasonable to expect that flow velocities relative to ambient flow velocities would increase with the vertical relief of an oyster reef. Bartol *et al.* (1999) discovered that mid-

intertidal oysters within reef interstices grow faster and live longer than oysters at the reef surface, and suggested that factors such as hydrodynamics vary between locations along the reef.

1.2 Sediment suspension, deposition and filtration on an oyster reef

Directly related to the hydrodynamics of an oyster reef is enhanced sedimentation due to active filtration of particles in the water column by the oysters and by the presence of reef structure. Too much sedimentation, however, can prevent larvae from attaching to shell and juvenile and adult oysters can be smothered. Sedimentation negatively affects recruitment and growth of oysters in the field, and sedimentation decreases with increased flow velocities (MacKenzie 1983). Oysters filter water to capture food such as phytoplankton and they filter sediment out of the water column at the same time. The sediment and seston the oysters remove from the overlying water column through active filtration (see Appendix I for preliminary study results) is then deposited on the benthic surface as pseudo-feces that are dense clumps of fine particles of sediment and organic material (Haven and Morales-Almo, 1966). Turbulent conditions created by the bed roughness improve resuspension of fine particles, and slowed flow velocity by the reef structure promotes sedimentation (Nelson *et al.*, 2004). Sedimentation is seasonally highest where flow speed is lowest at the bases of the reefs (Lenihan 1999), and sedimentation quickly covers low-relief reefs. In Lenihan (1999), his study identified the greater influences on oyster mortality. Macro-predators such as fish and crabs only accounted for 4-20% of total oyster mortality regardless of reef height, position, or cage type, whereas oysters at the base of reefs that were susceptible to burial by sediment

experienced greater mortality (97 ± 6%) than those on the reef crest (24 ± 9%). This supports the idea that physical-biological coupling has a great influence on the system.

1.3 Hydrodynamics of larval transport and settlement

Some challenges for oyster recovery efforts are promoting the successful larval transport to new reef sites, providing accommodating sites for larval settlement, and maintaining habitat suitable for oyster growth and survival. The topographic roughness and elevation of a reef are responsible for the local hydrodynamics that can impact the success of larval settlement and recruitment. Larvae preferentially settle on existing oyster reefs due to a hard, stable substrate for firm attachment and topographic variability that prevents burial by sediments. Settlement success has been shown to be dependent upon their ability to quickly land, attach, and undergo metamorphosis before they are washed away by fluid stresses, such as lift and drag, or are transferred to areas where they can be buried by depositing sediments. Shear stress acts tangential to their settlement surface and it is this shearing force that is capable of preventing settlement or dislodging the larvae after they settle (Reidenbach *et al.* 2009). Although previous studies have shown that benthic shear stresses influence the success of larval settlement (Soniat 2004), little is known about the actual distributions of shear stresses along oyster beds.

The physical structure of the reef controls physical variables such as flow speed which then determines the success of the oysters and oyster larvae in that location. Crimaldi *et al.* (2002) describes the link between local instantaneous bed shear stresses in a highly episodic stress record and the probability of successful settlement. This

experiment was in a laboratory with a bed of clams set equidistance apart from one another, and high resolution velocity measurements were used to infer stresses imposed on settling larvae. Not all of Crimaldi's conclusions can be applied to the densely populated oyster beds because the turbulence described occur between the clams shells with sufficient distance between each other may not exist in the small interstices between adult oysters. The observed transport of clam larvae to the bed, however, is likely similar to that of oyster larvae. Turbulence is not only responsible for the transport of larvae to the bed but can also be responsible for dislodging the larvae before they are permanently anchored. Clam larvae must land on the substrate during an adequately long stress lull to successfully anchor (Crimaldi *et al.* 2002), and higher Reynolds numbers meant that the larval fluxes to the bed were much greater. Instantaneous drag forces have been shown to be more likely to cause larval detachment than the maximum drag forces (Eckman *et al.* 1990).

1.4 Research questions

Based on the heightened focus on oyster restoration and necessity to defining parameters that will make restoration efforts more successful this study focuses on the role hydrodynamics plays in creating an environment that will encourage larval settlement success. The questions addressed through field research and laboratory flume experimentation are: (1) How do reef elevation and bed roughness affect shear stresses and fluid drag in the turbulent boundary layer over an intertidal oyster reef and adjacent restoration sites; (2) How does shear stress distribution and variability differ among sites

of varying topographies; and (3) How might the varying hydrodynamic conditions impact larval recruitment?

To address the first two questions, which will be discussed in Chapter 2, instruments were placed at an established oyster reef and adjacent oyster restoration sites located approximately 1 km offshore from the Anheuser-Busch Coastal Research Center at the VCR. The oyster site is part of a network of numerous healthy patches of oyster reefs surrounding an oyster restoration area operated by The Nature Conservancy. Work was in conjunction with restoration efforts being overseen by Barry Truitt, The Nature Conservancy (TNC) Director of Science and Stewardship at the VCR. First, the four study sites were surveyed which are adjacent to one another: the a healthy living reef, a TNC restoration site where the benthos was covered with fossil oyster shell to create substrate suitable for oyster larvae recruitment, a TNC restoration reef composed of whelk shell, and a site where the benthos is primarily composed of muddy sediment (Figure 2.1). The affects of elevation and roughness were found by measuring large scale velocity at three elevations on the healthy reef. Then, large scale velocity over the four study sites was measured to investigate how different bed topographies affect the local hydrodynamics.

The investigation of question 3, discussed in Chapter 3, required taking small scale measurements in the field and in a laboratory flume. First, the effects of bed roughness on the distribution of sheer stress were investigated by taking small scale velocity measurements over the same four study sites, mentioned above. Then the *in situ* measurements were coupled with laboratory measurements where a laser based particle

image velocimetry (PIV) technique was applied within a controlled laboratory flume environment to determine fine scale impacts of benthic roughness on shear stress distributions to mimic natural variability in roughness along oyster reefs. Shear stress is affected by benthic topography and flow dynamics, and the goal of this research was to quantify hydrodynamic processes affecting successful settlement of oyster larvae. The results of the flume studies allow for a more detailed examination of the small scale hydrodynamics that occur over a living oyster reef where larval settlement is known to be successful.

The the results of both large and small scale flow studies are meant to provide insight into the role hydrodynamics plays in providing an appropriate environment for growth and survivorship of oysters.

Chapter 2

Flow characteristics of an intertidal oyster reef and restoration sites

2.1. Motivation

The Nature Conservancy, in partnership with state and federal agencies is conducting large-scale efforts to restore eastern oyster populations in the Virginia Coast Reserve (VCR). One of the primary objectives is to increase suitable oyster habitat by adding hard substrate (fossil $CaCO_3$ shells) to the coastal bays adjacent to healthy reefs in the hope that natural recruitment processes will increase oyster biomass. These types of efforts have yielded encouraging results in some areas along the Virginia coastline (Coen and Luckenbach 2000).

To investigate hydrodynamic conditions that affect recruitment, both small-scale and large-scale flow studies were conducted over multiple benthic habitats. Within this chapter the focus is on the results of the large-scale flow field studies found by calculating hydrodynamic stresses, from velocity measurements, as they vary with elevation and among benthic structures.

2.2 Materials and Methods

2.2.1 Study Site

Studies were conducted within the Hillcrest reef tract, which is adjacent to the harbor located within the township of Oyster, VA (Figure 2.1) and is operated by The

Nature Conservancy (TNC). Instruments were deployed over an established oyster reef (HLCR2), a mud site (HLCR MUD), a restoration site made up of fossil shell collected from Sand Shoal Inlet (HLCR 2008), and a restoration site made up of whelk shell (HLCR WHELK). HLCR2 is considered a 'historical' reef because it has been an established reef since any kind of monitoring of the area began. The fossil shell that makes up HLCR 2008 was dredged out of Sand Shoal inlet, which is approximately eight miles east of Oyster, VA and between Cobb and Wreck barrier islands. The fossil shell was dredged and deployed during the summer of 2008. TNC is responsible for the naming scheme, division of the sites, and the fossil shell and whelk shell all laid at the site during the summer of 2008. Since the fossil shell and whelk shell are proving to have markedly different recruitment success, TNC is now monitoring them as separate sites.

Unharvested reefs such as HLCR2 are composed of tightly packed, vertically growing oysters. Recent restoration successes have been seen in sanctuary areas of the Chesapeake Bay where studies have found that the higher the vertical relief of the oyster reef, the more successful is the recruitment and growth of oysters (Schulte *et al.* 2009). Overall, a five-fold increase in living oyster densities was found, and attributed to the high relief of the successful oyster reefs. Hydrodynamic conditions over these reefs should be different than the hydrodynamic conditions over the low relief reefs because of factors such as water depth and benthic roughness. Lenihan *et al.* (1996) showed that the growth, condition and survival of oysters are positively correlated to an increase in flow velocity. It is reasonable to expect that flow velocities relative to ambient flow velocities would increase with the vertical relief of an oyster reef. Bartol *et al.* (1999) discovered

that mid-intertidal oysters within reef interstices grow faster and live longer than oysters at the reef surface, and suggested that factors such as hydrodynamics vary between locations along the reef.

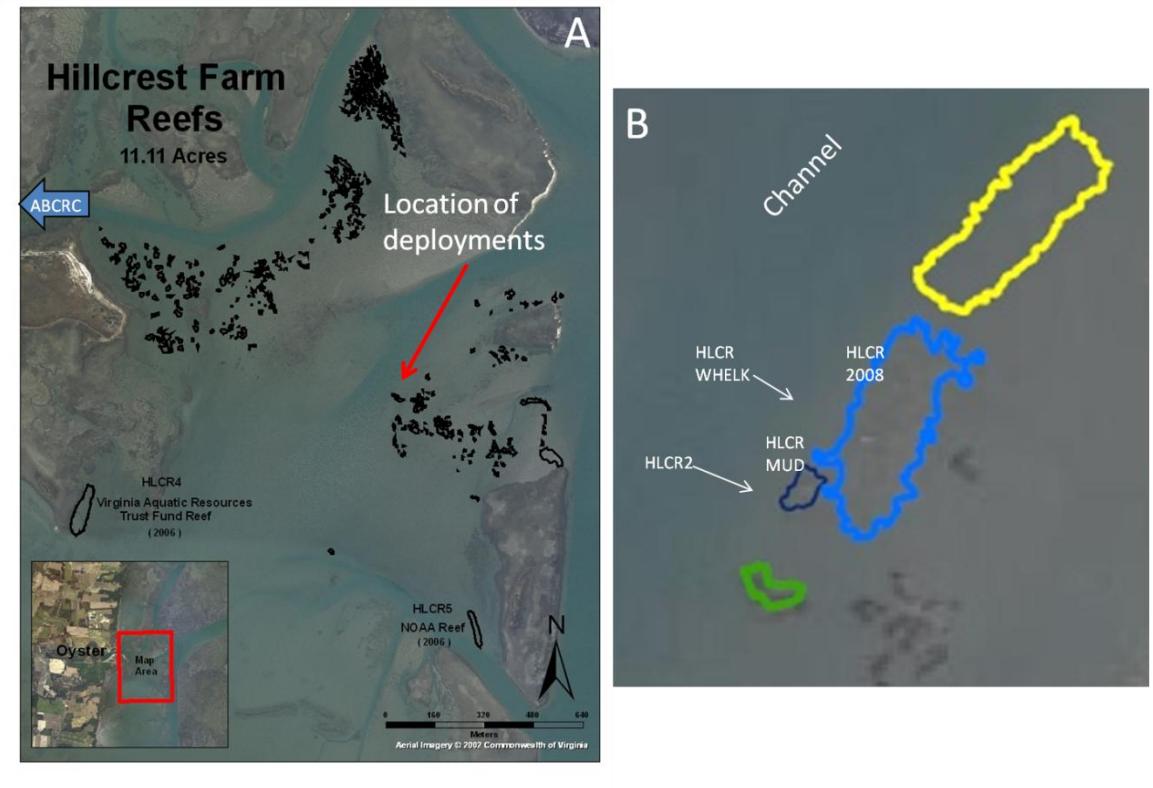

Figure 2.1: (A) Areal view of Hillcrest reef tract, the location of the Anheuser Busch Coastal Research Center and the location of the study site; (B) Specific deployment locations in relation to the channel as outlined by The Nature Conservancy

2.2.2 Elevation and roughness measurements

To define the elevation and benthic roughness, all sites were first surveyed to obtain relative elevations every 20 cm along multiple transects. A LaserMark LM800 Rotary Laser, with an accuracy of 1/16" at 100 ft, was placed on a tripod placed at a center point on the reef marked by an aluminum stake. HLCR2 was surveyed with 11

transects of varying lengths up to 15 m radiating from the center stake. The surveys of HLCR WHELK (Figure 2.2) and HLCR 2008 consisted of eight 6 m transects, and the survey of HLCR MUD consisted of four 6 m transects.

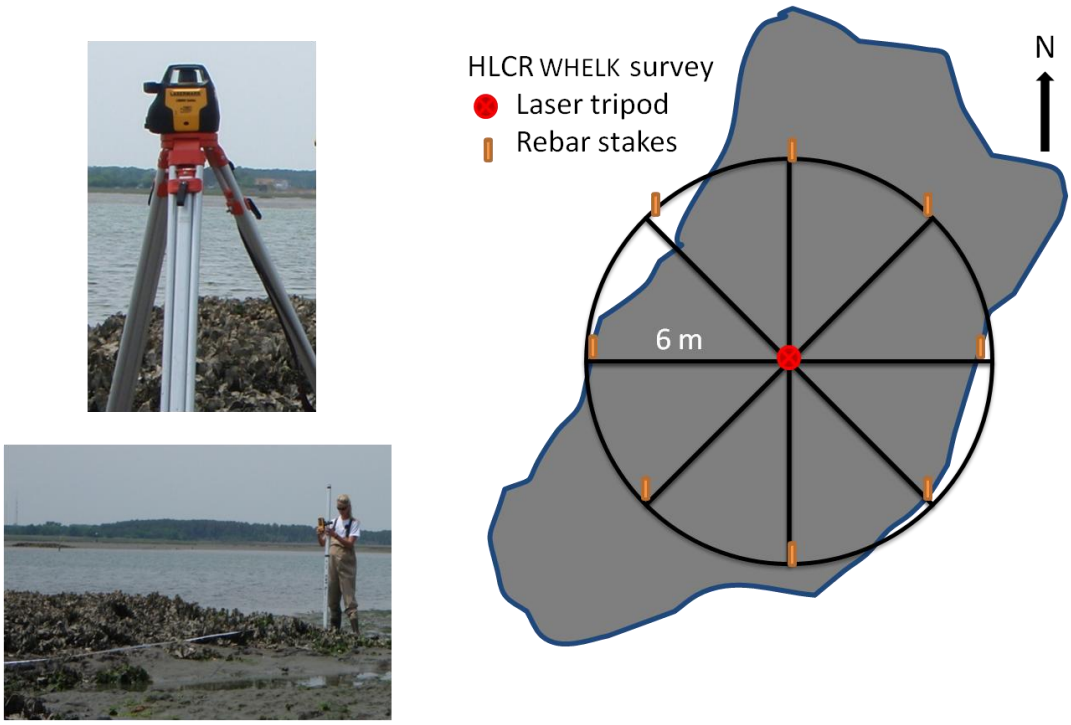

Figure 2.2: Top left: Laser Mark LM800 Series rotating laser mounted on a tripod; Bottom left: Taking elevation measurement with a stadia rod every 20 cm along the transect tape; Right: Location of 6 m transects on HLCR WHELK surveyed for elevation relative to the rotating laser eye mounted on a tripod in the center

Along each transect, the distance to the laser beam from the reef was measured every 20 cm using a hand held laser detector and a stadia rod. The 20 cm resolution was chosen to determine the variability and overall roughness differences between each site. With the height of the laser eye and distance from the laser to the ground at each stadia reading known, the relative elevations of each point were determined. The relative elevations were corrected by adjusting them according to a base point established using a

survey grade Trimble R8 GPS system. The Trimble R8 GPS unit has a horizontal accuracy to within 1 cm and a vertical accuracy from 2-3 cm. The Trimble R8 collected static observations of broadcasts from regional CORS base stations for approximately two hours in order to triangulate its exact position. Geoid09 was the model used for calculating elevation and the observations were processed using OPUS which is a commonly used method for this kind of GPS. Each data point from the laser lever survey was then adjusted to UTM NAD83, which is commonly used as a coordinate system and datum. The Trimble R8 was set at the center stake on HLCR 2008, and all elevations are relative to this datum unless otherwise specified. The instruments were deployed at the center origin of the surveyed transects. Elevations at the center point, relative to HLCR2, are: HLCR2: 0 cm, HLCR MUD: -37.16 cm, HLCR WHELK: -30.81 cm and HLCR 2008: -0.33 cm.

The four sites (Figure 2.1) differ in elevation by less than 40 cm. Sample transects of each site are illustrated in Figure 2.3. Here the differences in elevation are apparent, and a visual of the roughness differences at a 20 cm resolution is provided. HLCR MUD is the site found at the lowest elevation. HLCR 2008 is a mound of fossil shell that drops off in elevation away from the center. HLCR WHELK has a noticeable depression in the center where the instrument was placed and elevation increases towards the outside of the reef where mostly live oysters were observed. HLCR2 is relatively high in elevation at its crest and gradually decreases towards the surrounding mud flats and the channel. HLCR2 appears to have the greatest variability at the 20 cm resolution.

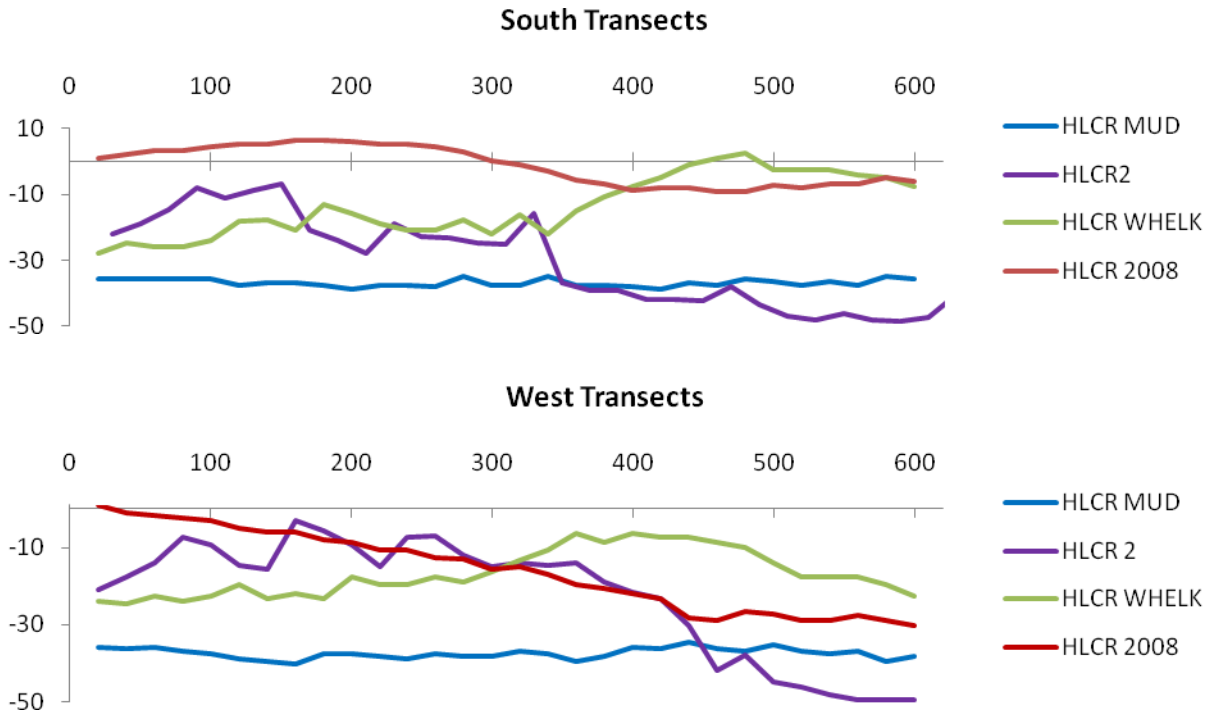

Figure 2.3: Transects of each study site from instrument location (0 cm) to the south (A) and west (B) for 600 cm.

To quantify the differences in roughness using the survey method an average elevation and standard deviation were calculated and plotted in Figure 2.4. HLCR2 has the greatest standard deviation, and mud has the lowest. HLCR 2008 has the second highest average elevation and standard deviation, but this is due to the way the fossil shell is deployed in mounds rather than smaller scale roughness elements.

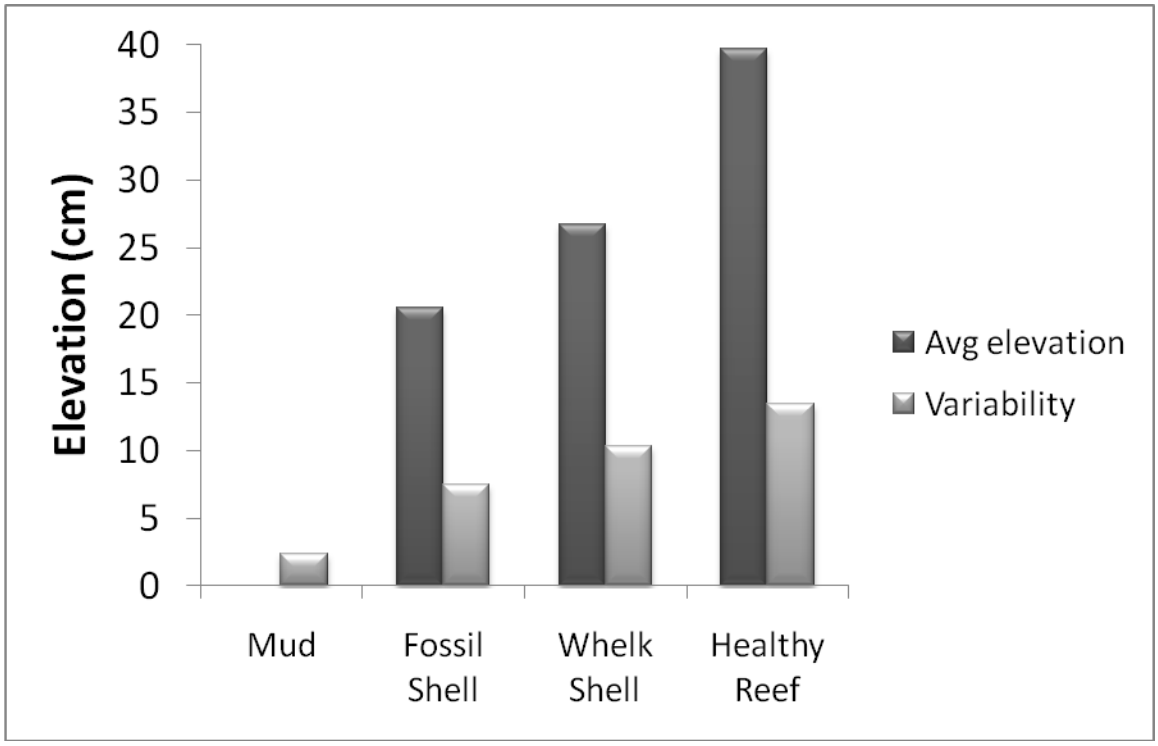

Figure 2.4: Elevations and topographic variability (standard deviation) relative to the HLCR MUD measured every 20 cm along 600 cm transects

2.3 Large scale hydrodynamics

2.3.1 Effects of elevation on flow and circulation

Three Nortek Inc.© Aquadopp Profilers (AQDPs) were deployed at three elevations on HLCR2 (Figure 2.5). The AQDPs have internal memory capacity and thus can be deployed autonomously for extended periods of time. Two of the AQDPs used in the elevation study are High Resolution (HR) and capture vertical profiles of the 3-dimensional velocities and mean flow patterns throughout the entire water column. The AQDPs capture velocities and mean flow patterns at a vertical resolution of 3 cm, a sampling rate of 32 Hz, and a horizontal velocity range of 30 cm s^{-1} (all adjustable

parameters). One other AQDP used was not a HR profiler, and collected velocities at a vertical resolution of 10 cm. The AQDPs were secured on frames constructed to sit on the seafloor and adjusted to minimize the tilt and role of the instrument.

The first AQDP (HR) was placed on the crest of the reef (HLCR_H) 75 cm above the mud floor, the second (HR) was placed midway up the reef (HLCR_M) 35 cm above the mud floor, and the third (not HR) was placed on the mud floor (HLCR_L) at the base of the reef. Oyster density and bed roughness was visually observed to be highest at OYST_H, moderate at OYST_M, and lowest at OYST_L. The three instruments were positioned along a line perpendicular to the main axis of the channel at a spacing of 3.65 m between instruments (Figure 2.5). Velocity profiles using the Vectrino were also taken adjacent to each of the AQDPs to profile the flow at a greater resolution and at a closer proximity to the substrate.

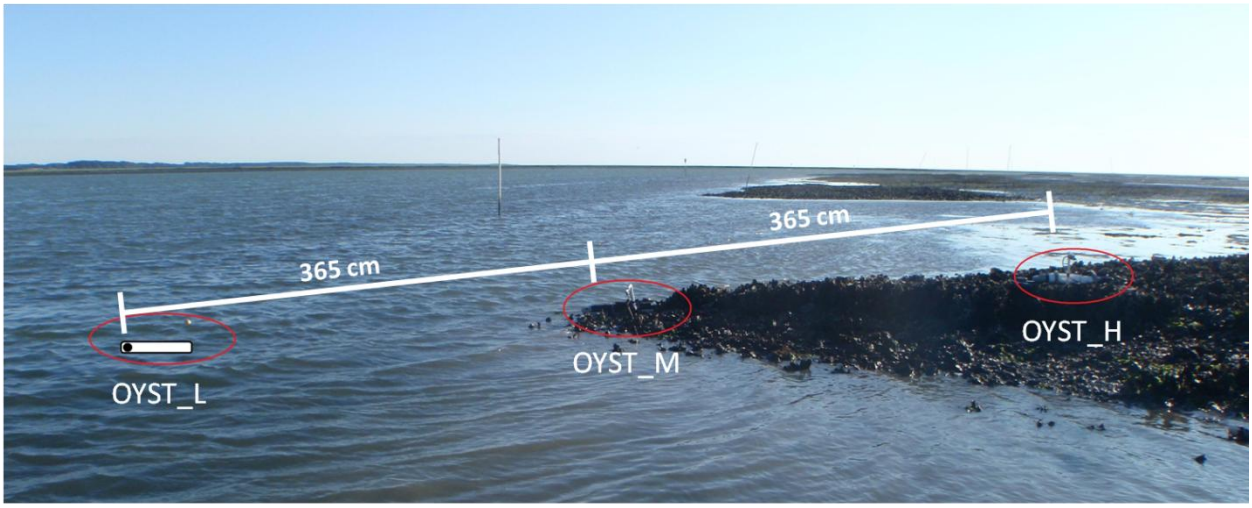

Figure 2.5: The three Aquadopps deployed for the Elevation Study were measured to be 365 cm from sensor to sensor. The elevation difference from OYST_L to OYST_M was 35.7 cm and from OYST_M to OYST_H was 39.5 cm.

The AQDPs at OYST_H and OYST_M were both HRs. They were set to sample continuously at a rate of 1 Hz and 3 cm bin resolution. The third AQDP at the base of the reef was on loan from Dr. Pat Wiberg and was not an HR and had less storage memory than the other two AQDPs deployed. The low resolution AQDP was deployed at the location with the deepest water column, OYST_L, where it could collect data from the greatest number of bins. The bins were set to the highest possible resolution, 10 cm, and the instrument collected data at a rate of 1 Hz for the maximum amount of time allowed given the limited memory. The start of data collection for this instrument was delayed by one half of a tidal cycle so that all three AQDPs were collecting data while micro-profiling of the flow adjacent to the reef was done using the Vectrino.

For the elevation experiment conducted on HLCR2, measurements were taken along a transect of increasing elevation across the reef. One difference between this study and those discussed above is the difference in tidal range. The previous studies by Lenihan et al (1996, 1999) and Schulte *et al.* (2009) were done along the dominant upstream-downstream flow direction in an estuary with a tidal range of only ~20 cm. The data collected during this experiment were taken across a transect perpendicular to the predominant direction of flow, during all tidal stages, with a tidal range of 1-2 m (Figure 2.6). Because of this difference and the asymmetric tides experienced in this area, velocity measurements were taken over five consecutive tidal cycles.

The instrument at OYST_L never comes completely out of water, whereas, the instruments at OYST_M and OYST_H do come out of water or are in water too shallow for data collection around low tides. For the purposes of comparison between sites, only

data collected when all instruments are collecting is considered. The AQDP at OYST_L were set to start data recording one tidal cycle later than the others because of its limited memory capacity. Water depth at OYST_L nearly reached 2 m, whereas depths at OYST_M and OYST_H did not rise above 1.5 m. The depths recorded at OYST_H are all slightly high due to the water being too shallow for the sensors to work properly. The depths used in calculations were adjusted based on observations taken while the instruments were deployed.

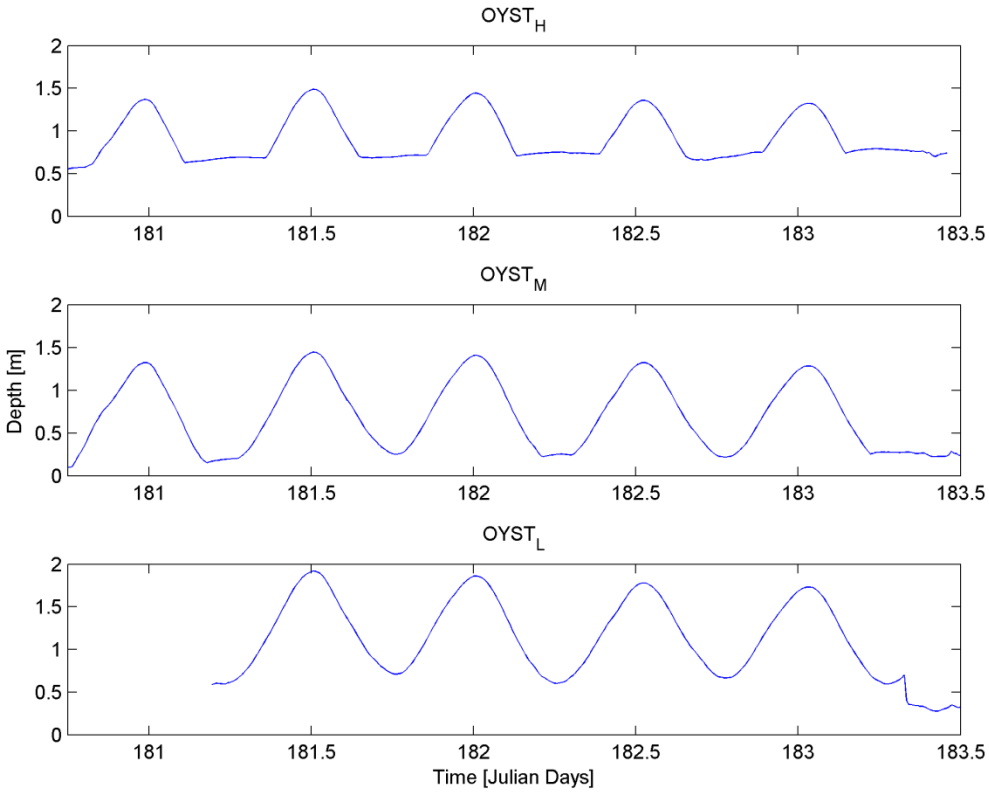

Figure 2.6: Mean depth as recorded by the three AQDPs simultaneously at the threeelevations over a period of three days.

Velocities were compared during different tidal stages such as flooding, ebbing, peak, and slack. A depth of 35 cm above the bed was analyzed across time for all AQDPs. This depth was chosen to allow for the blanking distance of the instruments and because it is a water column depth achieved at all sites for a decent amount of time across the tidal cycles. By doing this, differences in flow speeds can be analyzed independent of differing water column influences. Data collected by the AQDPs was processed to obtain vertical velocity profiles for the Up, North and East directions (See Appendix II), depth averaged velocity, and the horizontally averaged velocity. From the velocity data, shear velocity, u_*, and roughness length-scale, z_0, were calculated, using the "Law of the Wall" equation:

$$U(z) = \left(\frac{u_*}{\kappa}\right) ln\left(\frac{z-d}{z_0}\right), \tag{2.1}$$

where κ=0.41 is Von Karman's constant and d is the predetermined roughness height which is a vertical off-set to account for changes in elevation of the bed relative to datum. Because the flow in the benthic boundary layer is assumed to be turbulent and fully rough, the law of the wall can be used to appropriately describe the velocity profile (Cheng *et al.* 1999).

Due to surface reflections of the acoustic pulses in shallow waters, velocity records for the AQDPs are corrupted near the water surface and result in acceptable data collected for only the bottom one half of the water column over OYST_H. This surface reflection also accounts for the band of zero velocity in the third tidal cycle of OYST_H. Around day 182 during one tidal signal the AQDPs measured throughout the water

column. This was likely due to an extremely calm day and therefore the instrument recorded more accurate data closer to the surface.

High flow is observed at low and mid elevations before the water is deep enough to get data at the crest of the reef (Figures 2.7 and Appendix II).

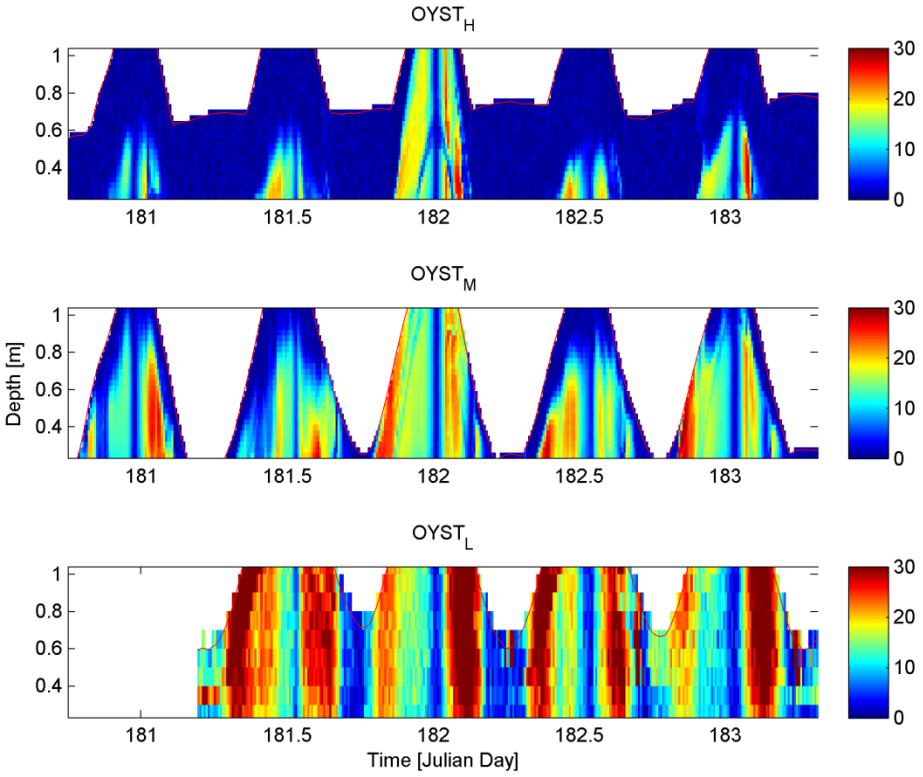

Figure 2.7: Horizontally averaged velocities over 5 consecutive tidal cycles taken simultaneously at 3 elevations

Horizontally averaged velocity magnitude (*U*) was calculated as the root mean square of the east and north velocities:

$$\sqrt{U_e{}^2 + U_n{}^2} = U \tag{2.2}$$

where U_e is east velocity, U_n is the north velocity, and U is the velocity magnitude (Figure 2.7). Depth averaged mean U for OYST_L, OYST_M, and OYST_H are 17.34, 7.68, and 2.75 cm/s respectively (Table 2.1). The drastic differences in depth averaged U between elevations appearing within color plots for OYST_M and OYST_H may be misleading, because feather plots show that the magnitude of velocity at an elevation of 20 cm is not drastically different between elevations (Figure 2.8).

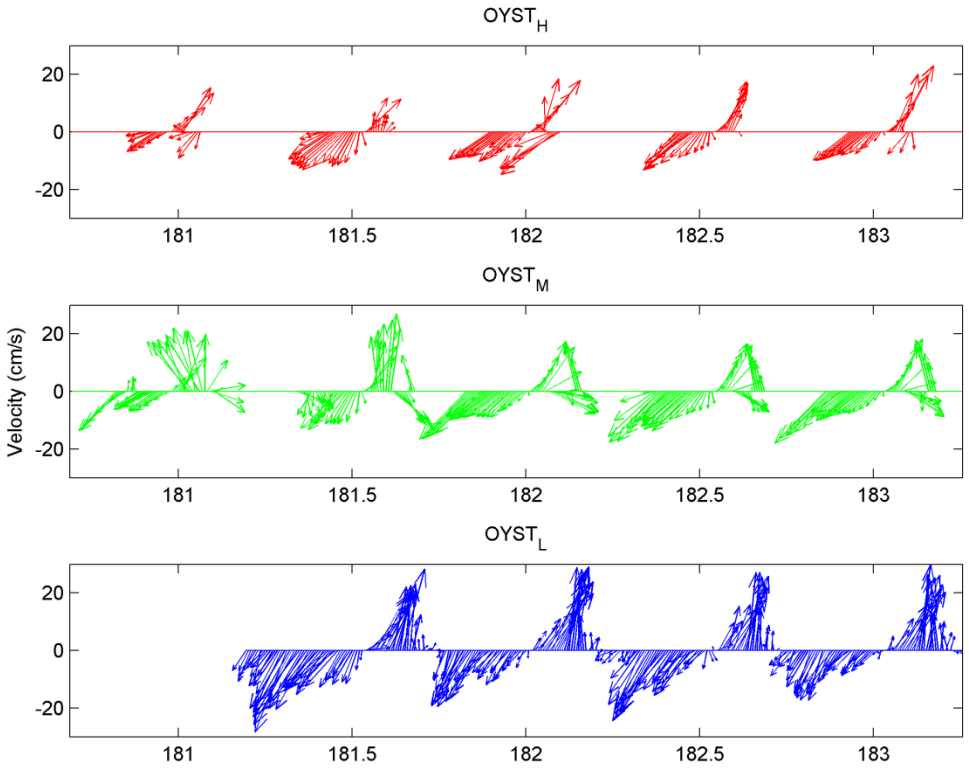

Figure 2.8: Feather plots of U at 20 cm above the substrate over five consecutive tidal cycles taken simultaneously at the three elevations

While the majority of the results can be attributed to local conditions (e.g. bed roughness at the point of measurement), some are linked to circulation patterns created by

the reef shape and changing tidal currents. Figure 2.8 displays velocity (20 cm above the bed) vectors over time and was created to look at flow direction rather than just velocity magnitude that has been used for most of the analysis thus far. Generally, except for slack tide, flow speeds are greater when the water is deeper. There appears to be a nearly instantaneous shift in flow direction over OYST_H, and little variation in magnitude, where the water is above the reef and not yet influenced by its shape. At OYST_M the change in flow direction is more gradual with a greater variation in magnitude. These differences can be attributed to large scale circulation patterns where water is forced around the reef as the tides flood and ebb.

Estimates of shear velocity (u_*), and roughness length (z_0) are obtained by regressing the velocity magnitude (U) on ln(z), where z is the height above the bed (Bergeron and Abrahams, 1992). As expressed mathematically in the "Law of the Wall" equation (Equation 2.1) U is dependent on ln(z). Shear velocity values were calculated only for vertical velocity profiles that conform to a logarithmic velocity profile with an R^2 value of 0.8 or greater (Figure 2.9). The log fit was calculated using water column heights of 0.50 m for OYST_H and OYST_M and 0.80 m for OYST_L instead of the commonly used 1.0 m height typically used (i.e., Reidenbach *et al.* 2006). Profiles that were eliminated because they were not logarithmic may have been taken during times of acceleration, deceleration, or high wind events (Gross and Nowell, 1983). Extremes in shear velocity can likely be attributed to high wind and wave action.

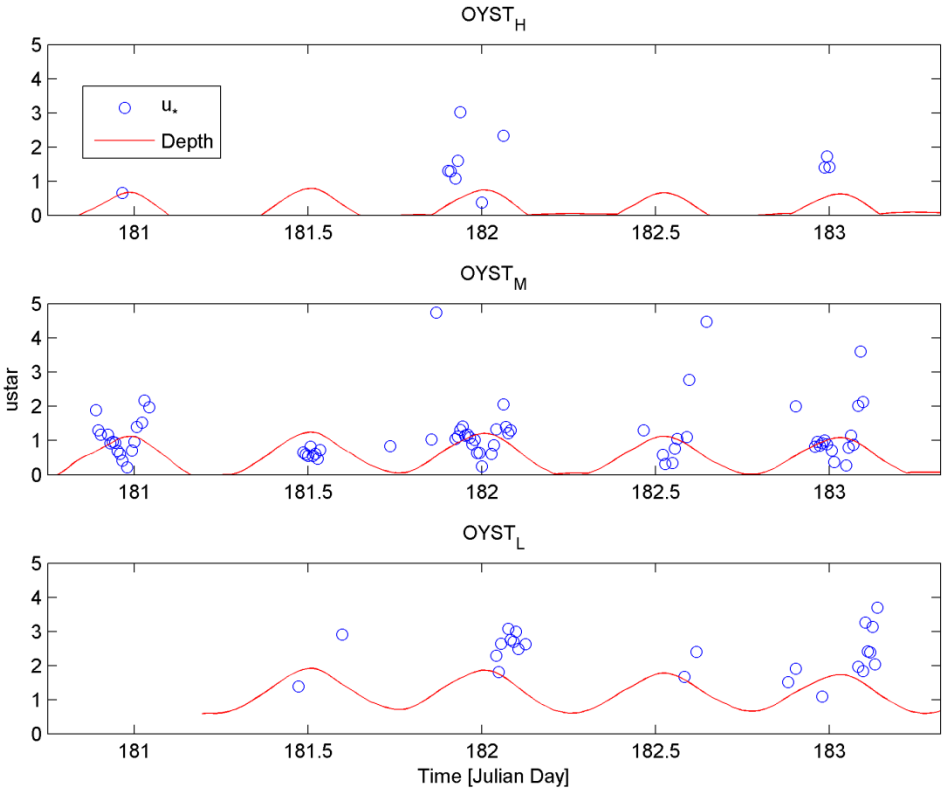

Figure 2.9: Depth plotted u_* at 35 cm above the substrate

Shear velocity, as well as *U*, at all elevations is greatest on either side of slack tide. The shallow water conditions and lack of a well defined boundary layer flow at OYST_H made the fitting of a log profile to the velocity data difficult. The AQDP at OYST_L was not a high resolution instrument, and therefore had fewer points to fit to the log profile. At OYST_M, however, the instrument was a high resolution AQDP in less shallow water. Here, a good number of vertical velocity profiles conformed to the logarithmic velocity profile, and thus it was reasonable to calculate a greater number of

u_* values. Figure 2.10 is a close-up of shear velocity and water depth during one tidal cycle.

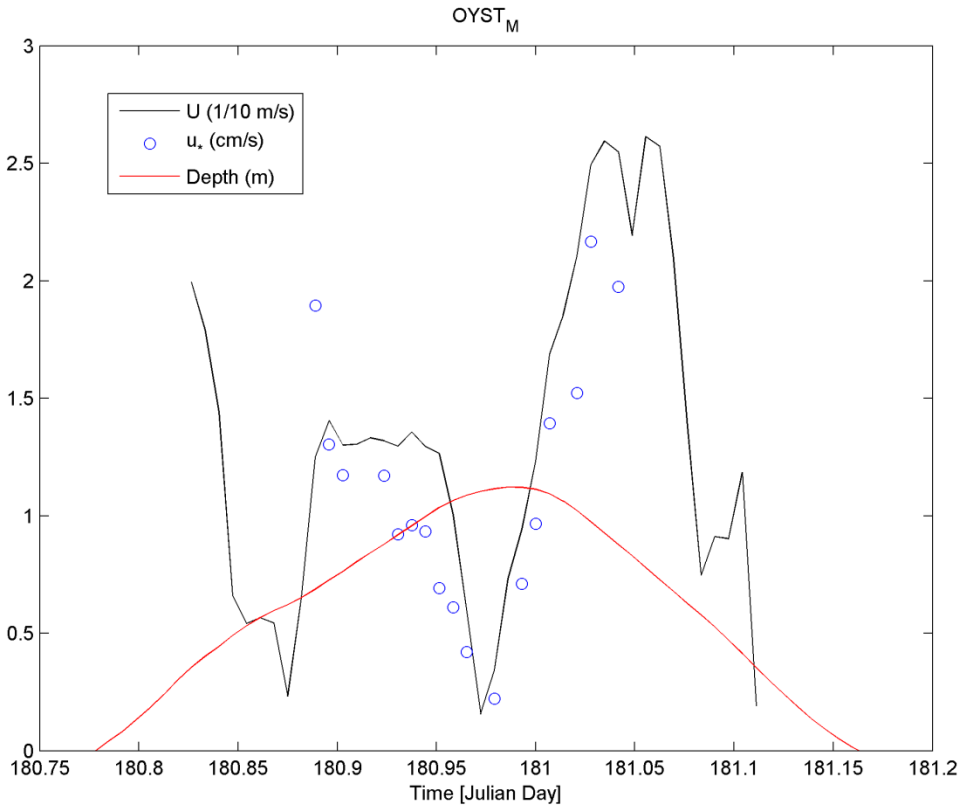

Figure 2.10: Depth plotted with U and u_* at 35 cm above the substrate to illustrate like trends; U was divided by 10 to show the general trends that u_* increases with mean U

Shear velocity trends towards 0 cm/s at slack tide, and increases with U during flood and ebb tides. Bottom shear stress can be expressed as

$$\tau_b/\rho = (u_*)^2 \qquad (2.3)$$

and is directly responsible for vertical mixing and sediment suspension and deposition (Cheng *et al.* 1999). For comparison between elevations mean and median u_* and z_0 are displayed in Table 2.1. Mean u_* for the entire measurement period is greatest, 2.37 cm/s, at OYST_L, lowest, 1.16 cm/s, at OYST_M and also relatively low, 1.47 cm/s, at OYST_H, so it is expected that sediment motion is greatest at the lowest elevation. The relatively greater u_* values correspond with greater velocities at OYST_L.

Location	Elevation (cm)	U_d (cm/s)	u_* Mean (cm/s)	z_0 Mean (cm)	C_D
OYST_H	76.2	11.36	1.47	0.96	0.015
OYST_M	40.0	13.42	1.16	0.30	0.0098
OYST_L	0.0	18.35	2.37	0.61	0.0088

Table 2.1: Calculation parameters and drag coefficients calculated using Equations 2.1 and 2.4 and a height from the bottom of 0.35 for OYST_H and OYST_M and 0.40 for OYST_L. U_d is the depth averaged velocity. Elevations are relative to the mud flat at OYST_L.

To quantify the drag experienced on the water flow by the benthic roughness at each location, a drag coefficient (C_D) was calculated to quantify roughness at each location (Reidenbach *et al.*, 2006):

$$C_D \equiv \frac{{u_*}^2}{{U_0}^2} \tag{2.4}$$

where U_0 is the instantaneous horizontally averaged velocity at an elevation of z = 40 cm above the bed. In agreement with visual observations (Figure 2.11), C_D increased with elevation: 0.0088 at OYST_L; 0.0098 at OYST_M; and 0.015 at OYST_H. The apparent trends of u_* decreasing with elevation and C_D increasing with elevation are opposite since

water velocity decreases near high tide and C_D is calculated directly from u_*. A displacement height (d_0) corrected for instrument placement relative to the surrounding vertical oysters at the highest elevation. At the lower two elevations live oysters were fewer and did not protrude into the water column above the instrument head. Peak drag occurs over the top of the reef with C_D=0.015. This is approximately 5 times greater than the canonical value of C_D=0.003 often reported for flows over muddy sites (i.e., Gross and Nowell, 1983). The drag coefficients are comparable to those found by Reidenbach *et al.* (2006) over a fringing coral reef.

Figure 2.11: Profile view of OYST_L, OYST_M, and OYST_H from right to left for a visual of roughness elements present around the instrument sensors

Total suspended solids concentrations (SSC) were estimated using OBS (Campbell Scientific OBS3+) at OYST_M and OYST_H (Figure 2.12). Similar to u_* trends, SSC is lowest during slack tides and greatest during times of high flow velocities, which occur during both flooding and ebbing tides. OBS data were included in Figure 2.12 and calculations of the 10-min means for times when the water column depth was 40 cm or greater. This conservative depth requirement was chosen to ensure wave action

(sensor coming in and out of water) did not impact the results. Mean SSC was 39.1 mg l^{-1} at OYST_H and 65.0 mg l^{-1} at OYST_M. The mean SSC during five full tidal cycles was more than one and a half time greater at the mid elevation than at the crest of the reef. At OYST_M the bed was a mix of live oysters, flat oyster shell, and sediment covered areas. At OYST_H the bed was all hard substrate composed of vertically growing live oysters with no notable sediment covered areas. The greater SSC observed at OYST_M may be a result of local resuspension and transport of the sediment observed at that elevation on the reef (Figure 2.11).

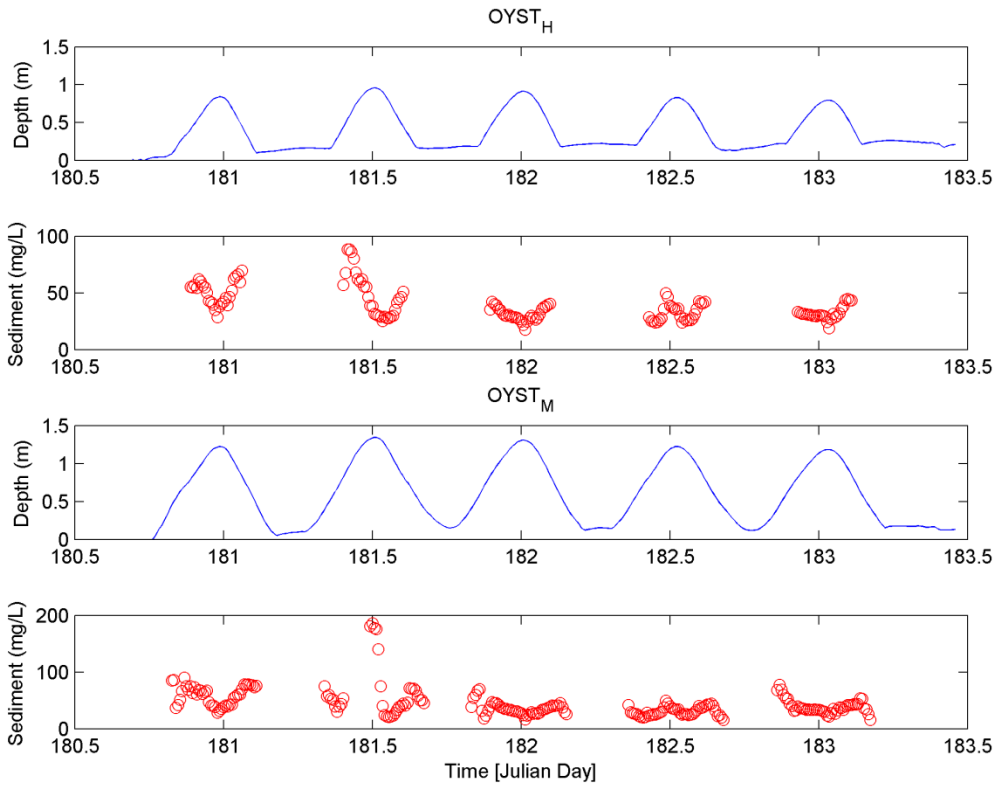

Figure 2.12: Suspended sediment plotted with depth for OYST_H (top) and OYST_M (bottom) during five consecutive tidal cycles

2.3.2 Hydrodynamics of various bed substrates: Multi-site study

With restoration efforts using different substrates (Figure 2.13) currently underway in the Hillcrest oyster track (Figure 2.1), where the study site is located, a comparison study of hydrodynamics over the different substrates was conducted to provide insight into how substrate impacts the varying success of restoration methods.

Figure 2.13: From left to right: HLCR MUD--mud, HLCR 2008--fossil oyster shell, HLCR WHELK--whelk shell, HLCR2--live oysters

A visual survey of the restoration sites, HLCR 2008 and HLCR WHELK, reveals many more living adult oysters growing on the whelk shell than on the fossil oyster shell (Also see Table 3.3 in the Recruitment study results).

For the multi-site study, four AQDP s were deployed at four different sites, all adjacent to one another, to measure velocity and mean flow patterns. The site names will be used to identify the AQDP deployments during this study. The first AQDP was placed on the historical (healthy) reef, HLCR2, the second was placed on HLCR WHELK, the third was placed on a mound of fossil shell within HLCR 2008 which, and the fourth AQDP was placed at HLCR MUD to get a bulk flow baseline (Figure 2.14). All AQDPs

were placed along and facing the channel for three consecutive days. The mud site, HLCR MUD, was used as the reference elevation of 0 cm, and above this were 36 cm at HLCR 2008, 6 cm at HLCR WHELK, and 35 cm at HLCR2. Vectrino measurements were taken adjacent to each of the AQDP s to profile the flow at a greater resolution and at a close proximity to the substrate. The deployment of the instruments was done as described above for the Elevation Study.

Figure 2.14: The four AQDPs deployed for the Multi-site study; (A) HLCR2, the historical reef; (B) HLCR WHELK, the whelk shell restoration site; (C) HLCR 2008, the fossil shell restoration site; and (D) HLCR MUD, the mud site between HLCR2 and HLCR WHELK; Note: In A, B, and C OBS are deployed with the AQDPs on PVC arms.

An AQDP and OBS were placed at the center of each site, the origin of the surveyed transects, so that the flow was affected by the local substrate for the maximum

distance considering the changing flow direction with the tides. The general tidal trends seen in the Elevation Study are the same for this study as well. The bulk flow results shown in Figure 2.15 are very similar to Figure 2.7.

The instruments, and surrounding substrate, were submerged for the greatest amount of time at the HLCR MUD because of it's relatively low elevation and was submerged for the least amount of time at HLCR2. The depths recorded at HLCR2 are all slightly high due to the water being too shallow for the sensors to work properly. Depths used in calculations were adjusted based on observations taken while the instruments were deployed.

Data was collected with the AQDPs in East-North-Up (ENU) coordinates, with dominant flow along the Northeast/Southwest direction parallel to the channel. Due to surface reflections of the acoustic pulses in shallow waters, velocity records are corrupted near the water surface and result in acceptable data collected for only the bottom one half of the water column over HLCR2 and HLCR 2008. Extremely calm surface conditions likely account for the times where it appears that the AQDP measure throughout the water column, such as in the fifth tidal cycle.

Flow velocities at all sites increase with depth during most tidal cycles and at all sights velocity drops to 0 cm/s at slack tide (Figures 2.15 and Appendix II). The instruments on HLCR WHELK and HLCR MUD were located at lower elevations than HLCR 2008 and HLCR2. The higher elevations experienced maximum velocity directly on either side of slack tide and typically for a time period less than 60 minutes. At the

two lower elevations, mean velocities near 20 cm/s were observed for several hours on either side of slack tide.

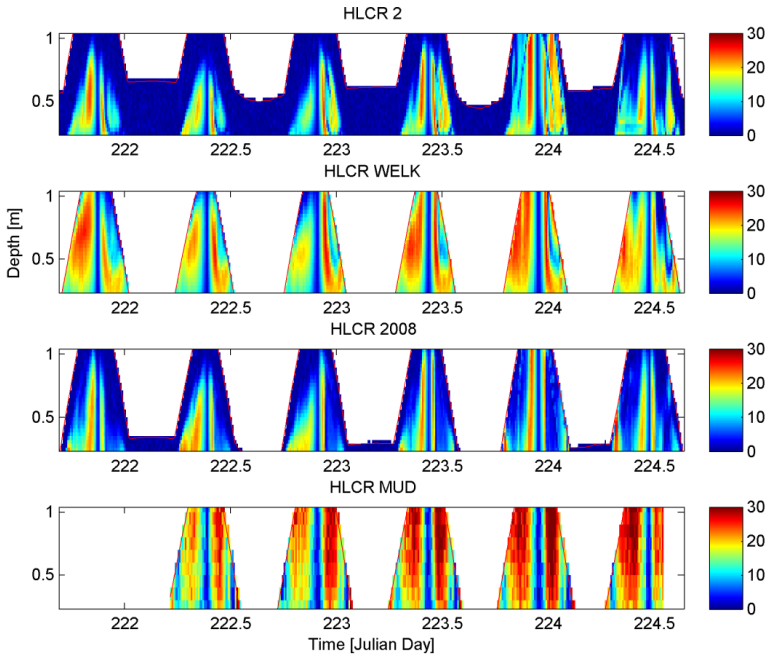

Figure 2.15: Horizontally averaged velocities over five consecutive tidal cycles taken simultaneously at the four sites

The depth averaged mean velocities (U_d) were recorded at HLCR2 and HLCR WHELK and were three and four times greater than those at HLCR 2008 and HLCR MUD. The mud site is located between HLCR WHELK and HLCR2, and the vertical relief of the adjacent reefs may be creating this low velocity zone over the lower elevation mud site. Having these low flow zones between reefs could be beneficial if sediment and resuspended pseudo-feces from adjacent reefs settles there instead of being carried onto reefs further downstream. Feather plots (Figure 2.16) show that the magnitude of velocity at an elevation of 20 cm is not drastically different between sites.

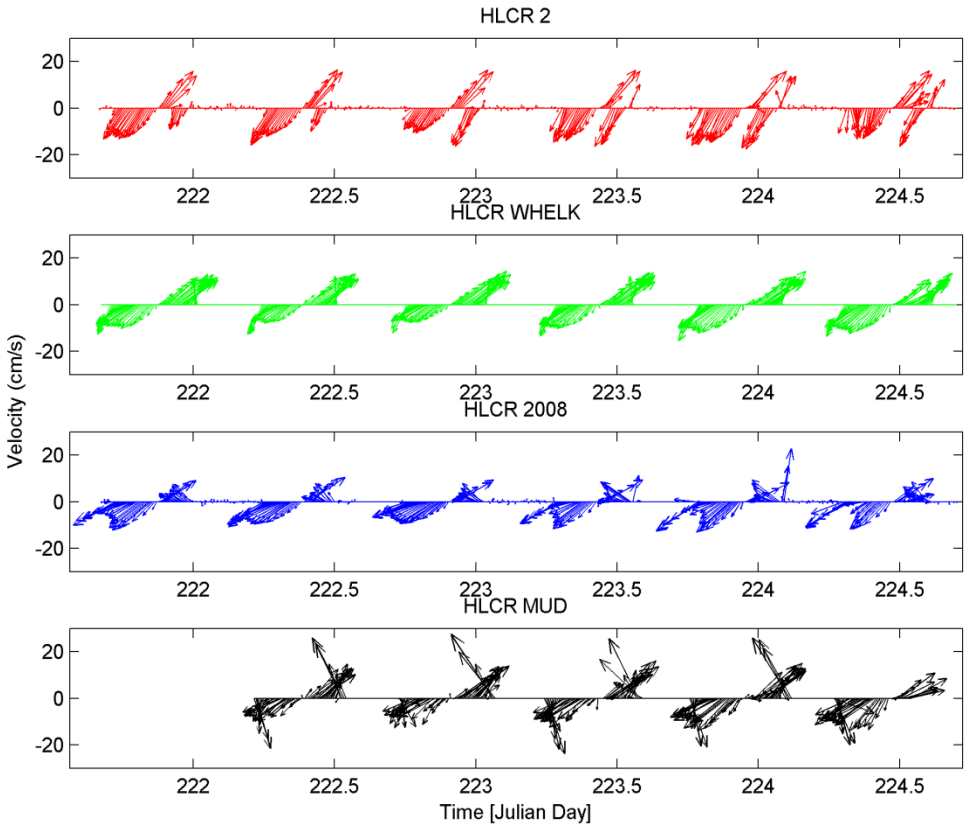

Figure 2.16: Feather plots of *U* at 20 cm above the substrate over five consecutive tidal cycles taken simultaneously at the four sites

The feather plots indicate mean flow parallel to the channel and reversing direction with tidal changes at all sites. At HLCR MUD, which is the last site to drain at low tide, the flow direction is toward the channel just before the AQDP comes out of water. This happens because this site is between HLCR WHELK and HLCR2 which block flow parallel to the channel from HLCR MUD below their elevations (Figure 2.1).

Location	Elevation (cm)	U_d (cm s^{-1})	u_* (cm s-1)	z_0 (cm)	C_D
HLCR2	37.2	11.7	1.23	0.28	0.015
HLCR WHELK	6.4	15.6	1.84	0.74	0.014
HLCR 2008	36.8	11.0	0.65	0.11	0.0026
HLCR MUD	0.0	18.5	1.72	0.33	0.0044

Table 2.2: Calculation parameters and drag coefficients calculated using Equations 2.1 and 2.4 and a height from the bottom of 0.35 for HLCR2, HLCR WHELK and HLCR 2008 and 0.40 for HLCR MUD. U_d is the depth averaged velocity, and elevations are relative to HLCR MUD.

C_D (Equation 2.4) for the various sites followed expectations with greatest magnitudes at HLCR2 and lowest at HLCR 2008. The vertical relief and high roughness of HLCR2 produced a relatively high u_* and caused U_d to be relatively low. At HLCR 2008 the vertical relief was also relatively high, so the shallow water conditions over the AQDP caused a low U_d. However, the lack of local roughness elements leads to a low u_* value. The drag coefficients are comparable to those found in the Elevation study discussed above and by Reidenbach *et al.* (2006) over a fringing coral reef.

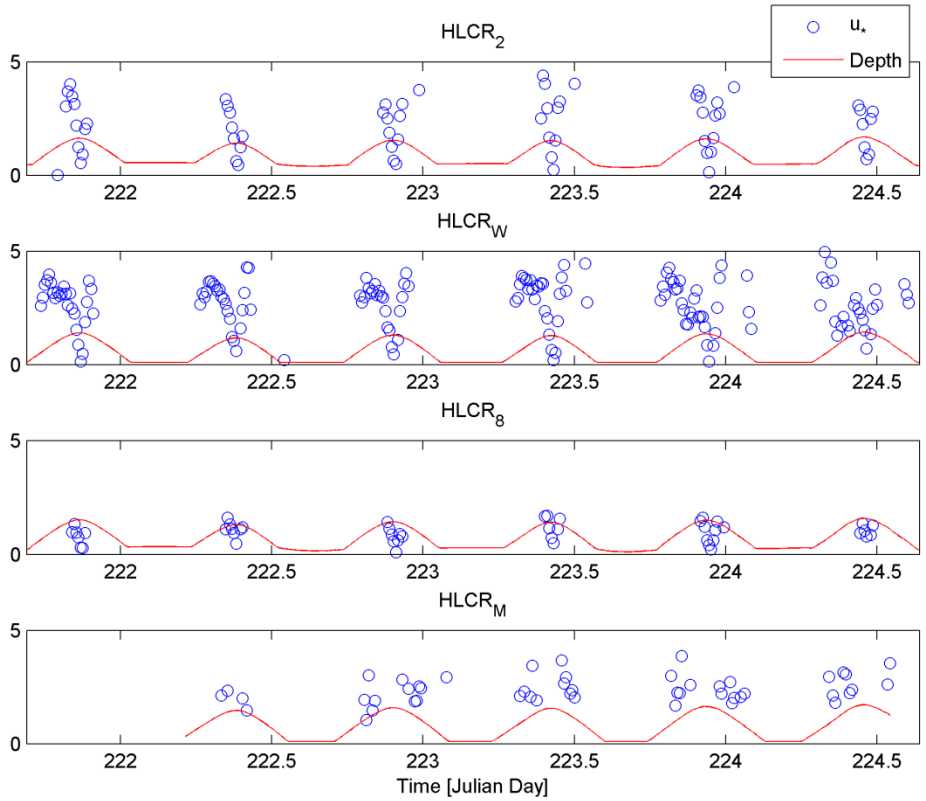

Figure 2.17: Depth and u_* plotted at 35 cm above the substrate over six consecutive tidal cycles

As observed in the Elevation study, the trend of increasing u_* with velocity recorded shortly before and after slack tide as the flow is decelerating and accelerating is also seen here. Depicted in Figure 2.17, u_* neared 0 cm/s during slack tides at HLCR2, HLCR WHELK, and HLCR 2008. However, at HLCR MUD the velocity profiles did not meet the requirement of having an R^2 value of 0.80 or greater at times of low flow so u_* was not calculated. This helps to explain why the mean u_* at HLCR MUD was greater than at HLCR2 and HLCR 2008.

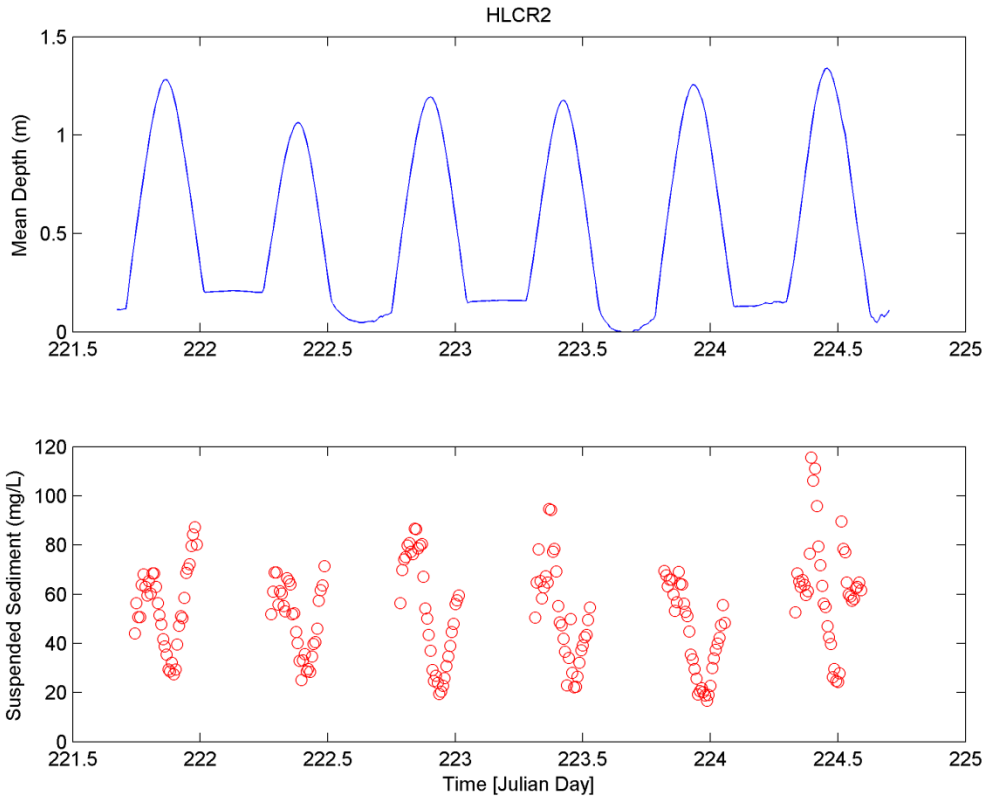

Figure 2.18: Suspended sediment concentration plotted at HLCR2 across six consecutive tidal cycles at times when water depth was greater than 20 cm

The OBSs were positioned 17 cm above the substrate at each site and the data was filtered to only include values when the water was greater than 40 cm deep (Figures 2.18-2.20). Similar trends to u_* are seen with relatively high concentrations observed shortly before and after slack tide, aligning with high flow velocities. However, differing from u_*, SSC increases during flood tides, but a mirrored decrease in SSC during ebb tides in not observed.

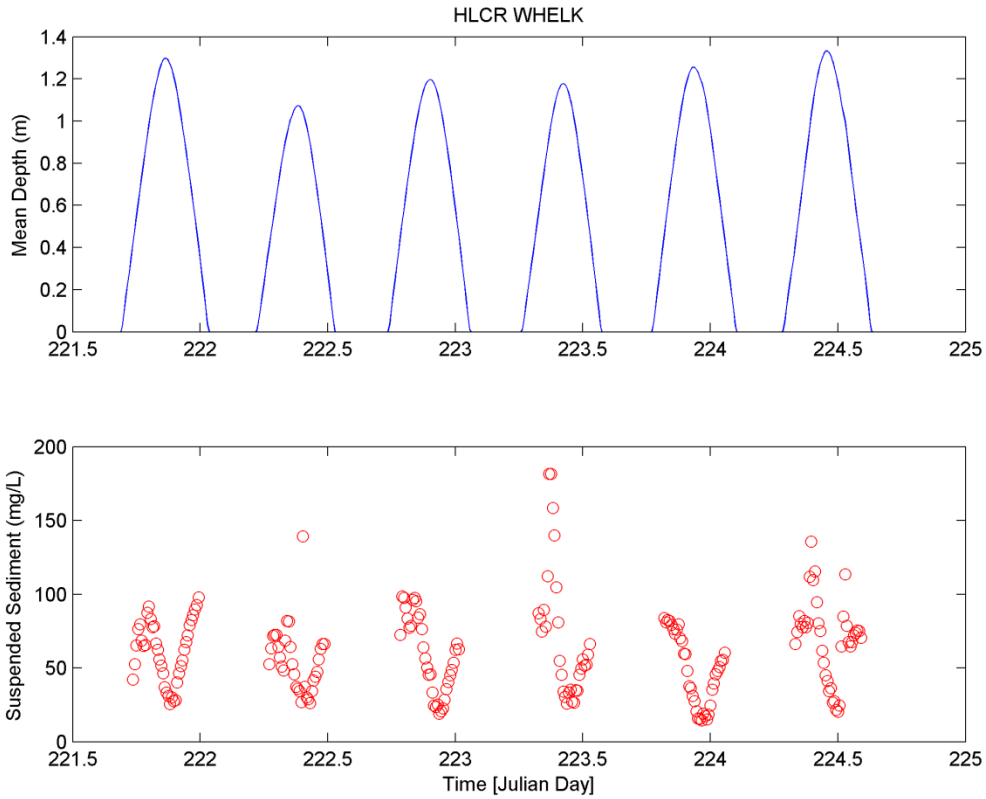

Figure 2.19: Suspended sediment concentration at HLCR WHELK plotted across six consecutive tidal cycles at times when water depth was greater than 40 cm

To compare SSC between sites, a mean sediment concentration value over the length of data collection period was calculated. Mean SSC was 53.2 mg l^{-1} at HLCR2, 62.7 mg l^{-1} at HLCR WHELK, and 64.3 mg l^{-1} at HLCR 2008 indicating that the bed of live oysters exhibited a decrease in sediment concentration. These results suggest that live oysters comprising a local area of hard substrate may contribute to the decrease in SSC due to their contribution to hard-substrate roughness and their active filtering (for preliminary sediment flux results refer to appendix I).

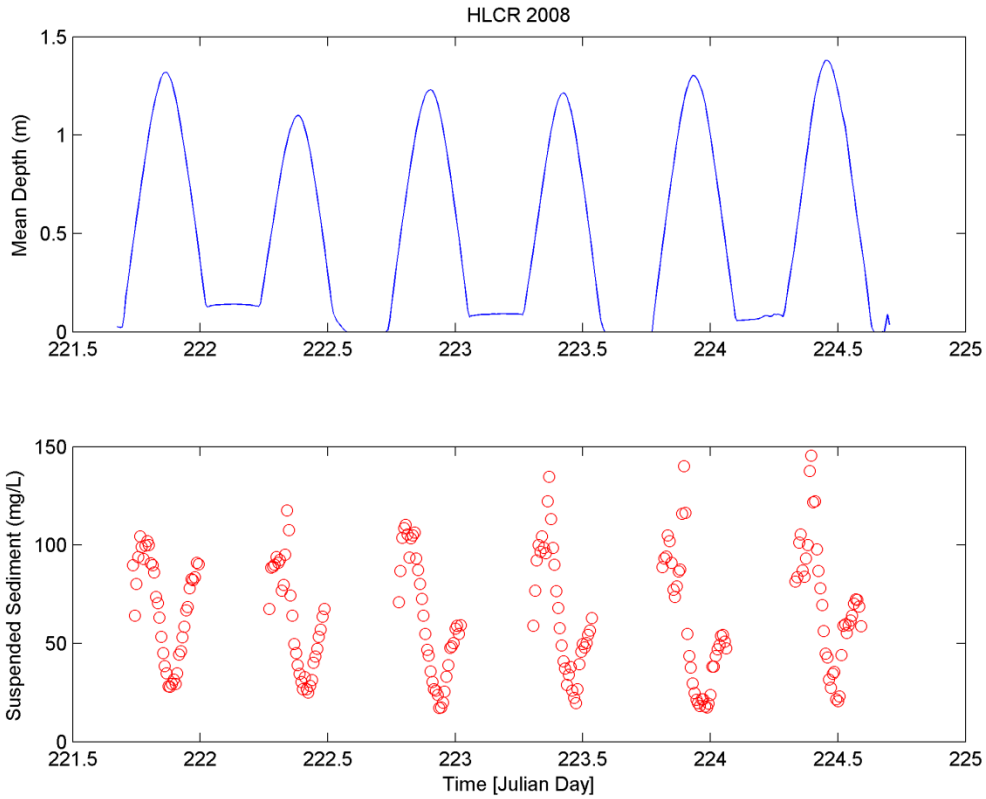

Figure 2.20: Suspended sediment concentration plotted at HLCR 2008 across six consecutive tidal cycles at times when water depth was greater than 20 cm

2.4 Discussion of large scale hydrodynamics

In the Elevation study the goal was look at how stresses differ with elevation to see if the results could help explain the results found by Schulte *et al.* (2009) and Newell (1999). They found that recruitment success increased with vertical relief, and in this study it was found that roughness increased and suspended solids decreased with elevation at HLCR2. Increased roughness not only increases the turbulence responsible for transport of oyster larvae to the bed (Koehl *et al.* 2007), it also provides areas of

refuge from predators (Soniat *et al.* 2004) and shear stress that could dislodge a larva before it attaches (Reidenbach *et al.* 2009).

In the Multi-site study the effects of bed roughness on the distribution of sheer stress were investigated by taking small scale velocity measurements over four sites adjacent to one another: a living reef, a whelk shell restoration reef, a fossil oyster shell restoration reef and a mud site. Large-scale velocities were measured over the same four sites to compare to the large scale flow patterns. Mean velocities decreased with elevation, while shear velocity appeared to be affected by the vertical relief of the site as well as local roughness. The drag coefficient did support the observation that HLCR2 and HLCR WHELK had greater roughness than HLCR 2008 and HLCR MUD. As in the Elevation study, mean suspended solids increased with observed roughness of the sites.

These results suggest that beds with greater elevation and roughness provide a better habitat for larval recruitment and growth than beds with lower elevation and roughness. In terms of the current restoration efforts being conducted by TNC, the whelk shell bed is a more suitable habitat for larval recruitment and growth than the fossil oyster shell bed.

Chapter 3

Structure Manipulation Study: Flume and Field

3.1 Motivation

Oyster larvae, like many other bivalve larvae, determine proper settlement sites depending upon local hydrodynamics (Koehl and Hadfield 2010). At the scale of oyster larvae, turbulence and fluid shear dictate hydrodynamic forces on larvae which have settled onto benthic surfaces. It has been observed in laboratory studies (Crimaldi *et al.* 2002, Koehl and Hadfield 2004) that certain hydrological conditions are ideal for larval settlement. Larvae preferentially settle where turbulent advection transports them to within the benthic boundary layer, on surfaces where shear stress is high, but once settled, where they have enough refuge from stresses to cement themselves to the substrate (such as in microhabitats or during lulls in near-bed turbulent stresses) (Crimaldi *et al.* 2002, Soniat 2004). Coupled with the benthic roughness of a living reef, larval transport to the bed is facilitated by turbulent mixing (Hendriks *et al.* 2006). The turbulence created by the morphology of an oyster reef not only brings food, such as phytoplankton, closer to the adult oysters but also transports oyster larvae to new settlment sites (Lenihan 1999). The turbulence transports the larvae to the bed, bringing them in contact with the benthos multiple times so that if they find their first landing site to be unsuitable they can release themselves back into the flow and test the next site they come in contact with (Fuchs *et al.* 2007; Soniat 2004).

In studies determining the impact of flow on oyster and barnacle larvae, settlement has been found to increase with velocity and shear (Bushek 1988; Soniat 2004), and barnacle larvae select local micro-sites with low shear (Wethy 1986). This low shear is often associated with crevices and narrow protective burrows that could be provided between roughness elements. Aimed at furthering this work, my study was designed to test how the position within a reef affects the instantaneous hydrodynamic forces experienced by *C. virginica* larva along settlement substrate of different geometric roughness.

To investigate these hydrodynamic forces, simplified structures of repeating and vertically oriented roughness elements were constructed and positioned within a laboratory flume. This study included flume studies of flow over 10 different benthic structures ranging from a flat bed to an idealized topography similar to that of an oyster reef. Five different bulk flow speeds were tested for each roughness, and a field study of recruitment on five replicates of three structure manipulations was also performed to determine how benthic roughness impacts recruitment success. Combined, both lab and field studies were used to determine the effects of benthic roughness on shear stresses and larval settlement.

3.2 Small-scale hydrodynamics in the field

3.2.1 Field Materials and Methods

Traditionally used in hydraulic laboratories, a Vectrino (Acoustic Doppler Velocimeter) was taken into the field to measure fine scale hydrodynamics between

tightly spaced live oysters *in situ.* The Vectrino was mounted on a stainless steel frame on an adjustable arm so that it could be raised and lowered to sample at the desired elevation. The Vectrino does not have internal memory storage capability, therefore data is transferred using a 30 m cable to a computer located on a boat moored just offshore of the reef. Velocity data was collected at 50 Hz for 10,000 samples at each elevation before the height of the instrument was adjusted. Velocity was measured at approximately 0.5, 1, 2, 3, 4, 5, 7, 10, and then 15 cm above the bed for each vertical transect (Figure 3.1). This measurement distribution was used so that there was greater resolution close to the bed where the small scale hydrodynamics and thus larvae are most affected by the roughness of the bed. The sampling volume for the Vectrino is defined by the intersection of the beams and is approximately 50 mm from the transmitter. For all profiles taken during the experiments, the sampling area was set to be 4 mm in diameter (user selectable) and 6 mm wide (fixed diameter) so that velocity data could be obtained extremely close to the substrate.

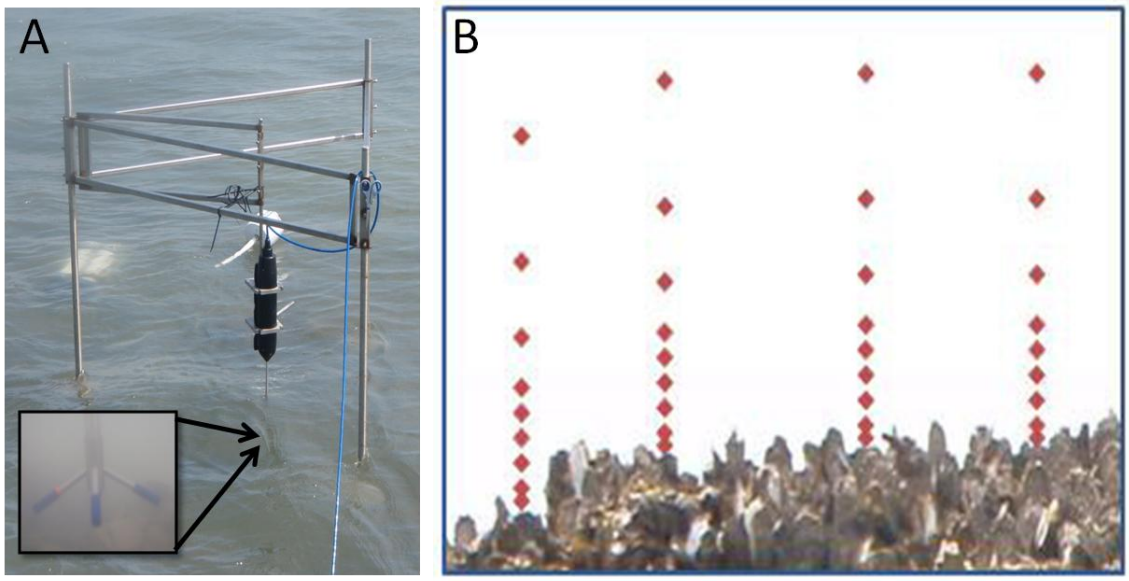

Figure 3.1: (A) The Vectrino recording point velocity measurements adjacent to an Aquadopp (underwater in the background); Inset: The Vectrino probe underwater and above oyster shell; (B) Each point represents the location where velocity data was collected (0.05, 1, 2, 3, 4, 5, 7, 10, and 15 cm above the substrate) using the Vectrino, and each column represents on vertical profile.

Velocity measurements were taken with the Vectrino over multiple vertical transects at randomized locations over the reef and restoration siteVectrino data was collected for 33 profiles over HLCR2 and five profiles over HLCR 2008. Data over the historical reef, HLCR2, was collected to determine the variability and distribution of shear stresses across an unharvested oyster reef. The data for the five profiles over the fossil shell site was taken to see what hydrodynamics are created over the same substrate with little or no vertical orientation. To maintain consistency between profiles taken over each site, all profiles included in the analysis have velocity measurements at an elevation of ~15 cm +/- 3 cm, and at an elevation <= 2 cm. All data above the point nearest to 15 cm was discarded to exclude wind affects near the surface. Concurrent with Vectrino

measurements, bulk flow was also measured using an AQDP placed on the crest of the reef and within ~1 m of where Vectrino measurements were taken.

Shear velocity, u_*, and roughness length-scale, z_0, were calculated from the Vectrino ADV profiles using the "Law of the Wall" (Equation 2.1) and Reynolds stresses were computed as the time average of the horizontal, u', and vertical, w', velocity fluctuations

$$\text{Reynolds stress} = \overline{u'w'} \tag{3.1}$$

The R^2 values for each profile were calculated to determine the goodness of fit to a logarithmic profile. The averages and standard deviations of points along the Reynolds stress and velocity profiles were calculated and plotted for further analysis and comparison of HLCR2 to HLCR 2008 hydrodynamics. Sample profiles (Figure 3.2) show peak Reynolds stresses ~2 cm above the bed at HLCR 2008 and ~6 cm above the bed at HLCR2. This implies that net momentum transfer, determined by velocity fluctuations, is greatest near the substrate at HLCR 2008 and over the tips of the oysters at HLCR2. Within the structure at HLCR2 Reynolds stress sharply decreases indicating an area sheltered from hydrodynamic stresses.

Displacement heights (d_0) were determined based on the mean elevation observed for all plotted profiles within each site where the profile started to assume a logarithmic fit. For the restoration site d_0 = 0 cm was used and for the healthy reef d_0 = 2 cm. To determine the closeness of fit to a logarithmic profile R^2 values were calculated using data at all elevations above the specified d_0. Profiles that did not fit a logarithmic profile

with an R^2 value of 0.80 or greater were discarded. Any profiles that did not conform to these parameters were not included in the comparison analysis.

3.2.2 Field velocity profile results

At the restoration site (Table 3.1), HLCR 2008, u_* values ranged from 0.47 cm s^{-1} to 3.37 cm s^{-1} with a mean of 2.05 cm s^{-1}, a standard deviation of 1.31 cm s^{-1}, and a median of 1.93 cm s^{-1}. The z_0 values ranged from 0.11 cm to 0.45 cm with a mean of 0.24 cm, a standard deviation of 0.13 cm, and a median of 0.20 cm. At the healthy reef (Table 2.1), HLCR2, u_* values ranged from 0.69 cm s^{-1} to 4.41 cm s^{-1} with a mean of 1.90 cm s^{-1}, a standard deviation of 1.05 cm s^{-1}, and a median of 1.78 cm s^{-1}. The z_0 values ranged from 0.00 cm to 1.66 cm with a mean of 0.35 cm, a standard deviation of 0.50, and a median of 0.09 cm. Reynolds stresses were also normalized using the equation:

$$R = \frac{\overline{u'w'}}{U^2} \tag{3.2}$$

where the time average of the horizontal, *u'*, and vertical, *w'*, velocity fluctuations are divided by square of the mean velocity magnitude, *U*, at the top (elevation of ~15 cm) of each respective profile (Table 3.1).

Site	Reef Type	Statistic	Elevation above reef (cm)	Normalized Reynolds Stress	u_* (cm s^{-1})	z_0 (m)	R^2	d_0 (cm)
HLCR 2008	Restoration	Mean	15.1	0.0029	2.05	0.24	0.93	0.00
HLCR2	Healthy	Mean	15.4	0.0076	1.90	0.35	0.89	2.00
HLCR 2008	Restoration	Median	14.6	0.0012	1.93	0.20	0.93	0.00
HLCR2	Healthy	Median	15.1	0.0059	1.78	0.09	0.89	2.00
HLCR 2008	Restoration	Min	14.0	0.0003	0.47	0.11	0.85	0.00
HLCR2	Healthy	Min	13.9	0.0004	0.69	0.00	0.80	2.00
HLCR 2008	Restoration	Max	16.7	0.0107	3.37	0.45	0.99	0.00
HLCR2	Healthy	Max	18.6	0.0353	4.41	1.66	0.95	2.00
HLCR 2008	Restoration	Stdev	1.1	0.0044	1.31	0.13	0.05	0.00
HLCR2	Healthy	Stdev	1.15	0.0087	1.05	0.50	0.04	2.00

Table 3.1: Means and medians from five profiles taken over HLCR 2008 and 16 profiles taken over HLCR2; these are the profiles that conformed to a logarithmic profile with an $R^2 > 0.80$. Note: The normalized Reynolds stress values are the absolute value of the mean velocity magnitude at the point nearest to 15 cm above the reef.

Both shear velocity, u_*, and roughness length-scale, z_0, increased with an increase in bottom roughness and topographical variability. For example, the healthy reef is composed of tightly packed and vertically oriented live oysters, whereas the restoration site comprises horizontal halved fossil oyster shells. By observation it is easy to see that bottom roughness and topographic variability increases from the restoration site to the healthy reef. Median values for both u_* and z_o are higher for the healthy reef than the restoration site. The enhanced roughness also allows for regions of slower flow and reduced turbulence between individual oysters. Although mean u_* and z_0 values do increase from restoration site to healthy reef, however, they are not significantly different ($\alpha = 0.05$, P-value: 0.80). Greater differences are possibly not seen because the oysters are so tightly packed on the healthy reef the local flow skims over the top instead of being largely affected by the roughness.

Representative profiles have been chosen for each study site and a mud bottom site, HLCR MUD, to further explain and illustrate the hydrodynamics created by the differences in bottom roughness. The representative velocity profiles are plotted along with normalized Reynolds stress (Figure 3.2). The Reynolds stress was normalized using the velocity nearest to 15 cm above the substrate (Eq. 3.2). The Reynolds stress over the HLCR2 peaked at an elevation of approximately 6 cm, which is the height of the oysters for this profile and where the velocities begin to assume a logarithmic profile. At HLCR 2008 the Reynolds stress peaks at around 2 cm from the substrate suggesting that there is less shelter from the hydrodynamic forces such as lift and drag that could prevent settling of oyster larvae. Reynolds stresses peak at all sites when velocity is 9-11 cm s^{-1}.

Enhanced roughness creates regions of high turbulence above the bed and lower turbulence and velocities within the bed structure. At the top of the reef, a strong shear layer develops within the velocity profile which enhances momentum transport to the bed. Over HLCR MUD the peak in Reynolds stress is seen at the elevation where an inversion in the velocity profile occurred. At HLCR 2008 Reynolds stress peaks at -0.006 cm^2 s^{-2} and is nearly double the peak of -0.0025 cm^2 s^{-2} found at HLCR2 and HLCR MUD. The greater Reynolds stress found adjacent to the substrate at HLCR 2008 means greater net momentum transfer at the substrate surface that could enhance shear acting on the larvae and enhance larval dislodgement (Reidenbach *et al.* 2009).

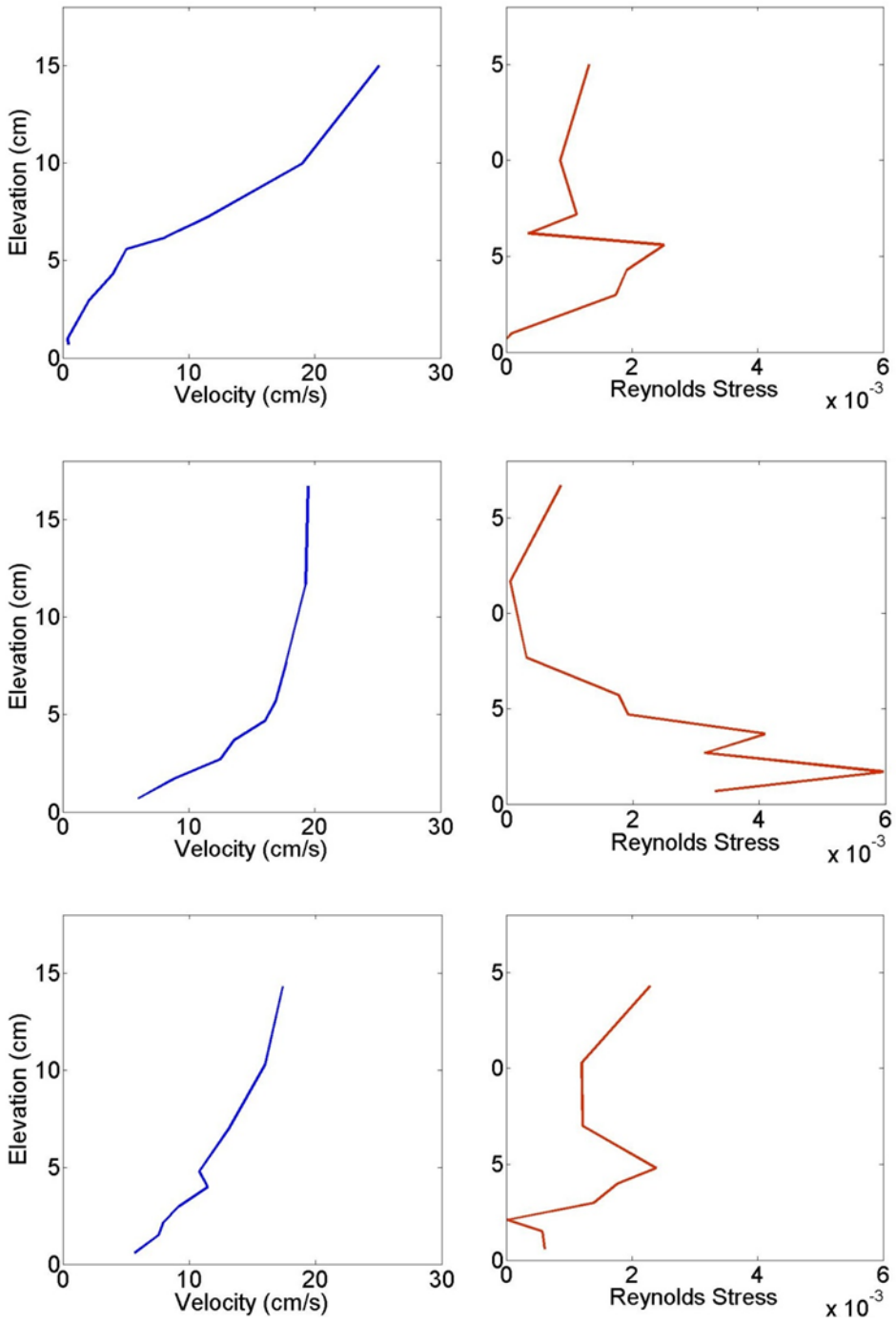

Figure 3.2: Horizontally averaged velocity profiles cropped above point nearest to 15 cm and corresponding normalized Reynolds stress profiles for (top) healthy reef, (middle) restoration site, and (bottom) mud site. Note the elevation where Reynolds stress peaks is much higher for the healthy reef than for the restoration site.

To further describe how turbulent fluctuations contribute to momentum distribution throughout the bottom boundary layer (Lu and Willmarth 1973, Luckhik and Tiederman 1988) quadrant analysis was performed. To perform quadrant analysis, u' and w' velocity fluctuations are divided into four quadrants based on the sign of their instantaneous values. Contours of the turbulent probability distribution function (pdf) are shown in Figure 2.5 for turbulence 6 cm above the reef. In quadrant 1 (Q1), $u' > 0$, $w' > 0$, in Q2, $u' < 0$, $w' > 0$ (a turbulent ejection), in Q3, $u' < 0$, $w' < 0$, and in Q4, $u' > 0$, $w' < 0$ (a turbulent sweep). Sweeping events, illustrated by pdf values in Q4, transport high momentum fluid downward towards the reef. Pdf values in Q2 illustrate ejection of low momentum fluid vertically upwards away from the reef. These ejection and sweep events result in intermittent flushing of "dead water" that accumulates among roughness elements (Grass 1971). Growing oysters depend on this flushing to replace seston depleted water with water containing food. Momentum transport is typically dominated by these ejection and sweeping events and in this case show up in Q2 and Q4. This is true for flow over the reef (Figure 3.3), where Reynolds stress factors are dominated by motions within Q2 and Q4.

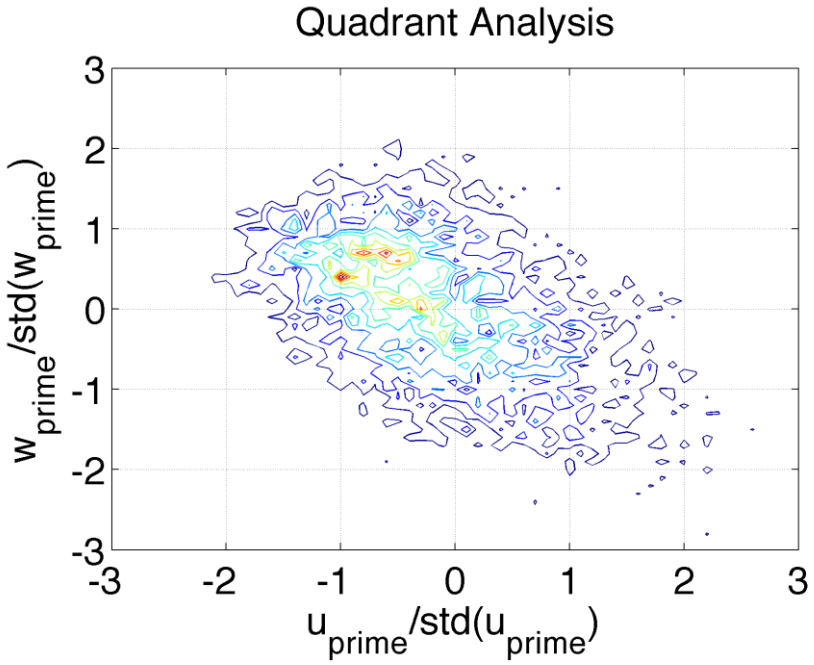

Figure 3.3: Quadrant analysis of velocity fluctuations located 6 cm above the healthy oyster reef.

The total contribution to the Reynolds Stress within each quadrant was found by summing the *u'w'* contributions: Q1 (8%), Q2 (33%), Q3 (7%), and Q4 (51%). The combined Q2 and Q4 contributions account for approximately 84% of the total Reynolds stress, which is similar to results found by other studies of flow over high roughness topography (Bennet and Best 1996; Lacey and Roy 2008). Q4 events dominate overall; indicating that the turbulent sweeps of vortices of high energy eddies reaching into the oyster reef dominate the contribution. For the HLCR 2008, there is a more even balance of ejection and sweep events (Figure 3.4), with contributions of the quadrants of: Q1 (9%), Q2 (44%), Q3 (10%), and Q4 (37%).

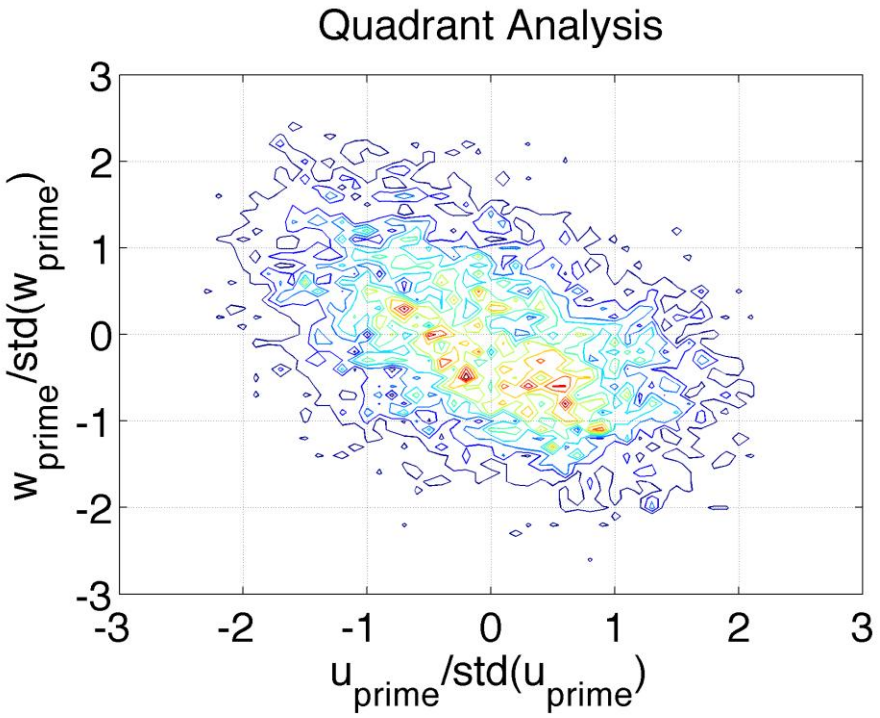

Figure 3.4: Quadrant analysis of velocity fluctuations found 6 cm above the restoration reef.

These results suggest that larvae and food carried by high momentum fluid are swept down to the reef more frequently at HLCR2 than at HLCR 2008. This also suggests that there is potential for higher rates of larval settlement at HLCR2 simply because of the higher frequency of larval delivery to the substrate. Growing oysters at HLCR2 are also provided with food by these sweep events. Even though ejection events occur more frequently at HLCR 2008 than at HLCR2, flushing still occurs at HLCR2 to ejection of "dead water" between growing oysters (Grass 1971).

3.3 Small-scale hydrodynamics in the field

3.3.1 Laboratory Materials and Methods

The laboratory-based flume study quantified specific hydrodynamic forces such as lift, drag, and turbulent bed shear stresses acting along different surfaces adjacent to an oyster bed that may impact larval settlement. Experiments were conducted within an open channel recirculating water flume (Figure 3.5), designed based on schematics by Tamburri *et al.* (1996). The flume used in the Tamburri et al. (1996) studied dissolved chemical cues inducing the settlement of *Crassostrea virginica* larvae (Jonsson *et al.* 2006) and was therefore considered a useful flume for micro-scale turbulence studies. The flume was constructed using Lexan ™, a polycarbonate resin thermoplastic, to be 20 cm wide, with 20 cm high walls, with semicircular ends of radius 40 cm and with two straight sections 100 cm long. One straight section is fitted with a glass pane for photo-image clarity and the motor and flow generation system are fitted in the opposite straight section. Two additional, yet thinner sheets of Lexan ™ were placed within each curved section of the flume parallel to the walls to minimize turbulence and secondary flow conditions created as the flow moves around the curves. The design for the flow generation system uses 12 inch LP records mounted to a shaft, perpendicular to the flow, on a motor with a speed controller. This system uses frictional drag to drive the flow, rather than propulsion from a propeller, creating the appropriate channel flow velocities without causing lethal damage to organisms (which may be used in future research) within the flume. The different mean channel flow conditions were created by adjusting

to a range of velocities comparable to velocities observed at the field site (approximately 5-25 cm/s).

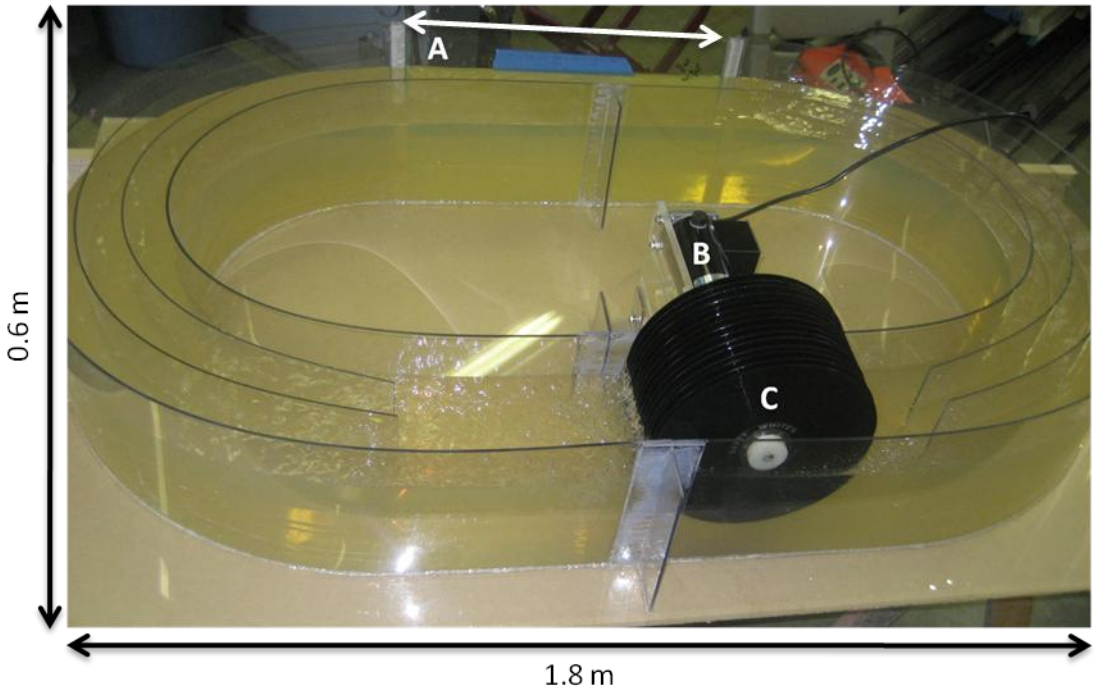

Figure 3.5: Recirculating water flume: A) Glass imaging section; B) Motor attached to a speed controller; C) Rotating long play (LP) vinyl records spaced vertically 1 cm apart to generate flow

To mimic benthic roughness that impacts flow and turbulence, an adjustable benthic structure was constructed from Plexiglas pieces cut to the width of the flume (20 cm) by eight cm (Figure 3.6). The pieces were hinged together in an accordion style using piano hinges cut to the length of the Plexiglass pieces. The hinges were attached using silicon glue and reinforced with duct tape. To prevent reflection of the laser used for velocity studies, a black multipurpose spray paint was used to coat the entire structure. As the peak spacing increased the peak heights correspondingly decreased from

an initial 8.5 cm at the smallest peak spacing to 4.7 cm at the greatest peak spacing. To prevent water column depth becoming a factor, the peaks were raised by putting additional Plexiglas pieces under the structure as spacers as the peak heights decreased. The depth from the surface of the peak heights was maintained in this way within a range of 11-12 cm.

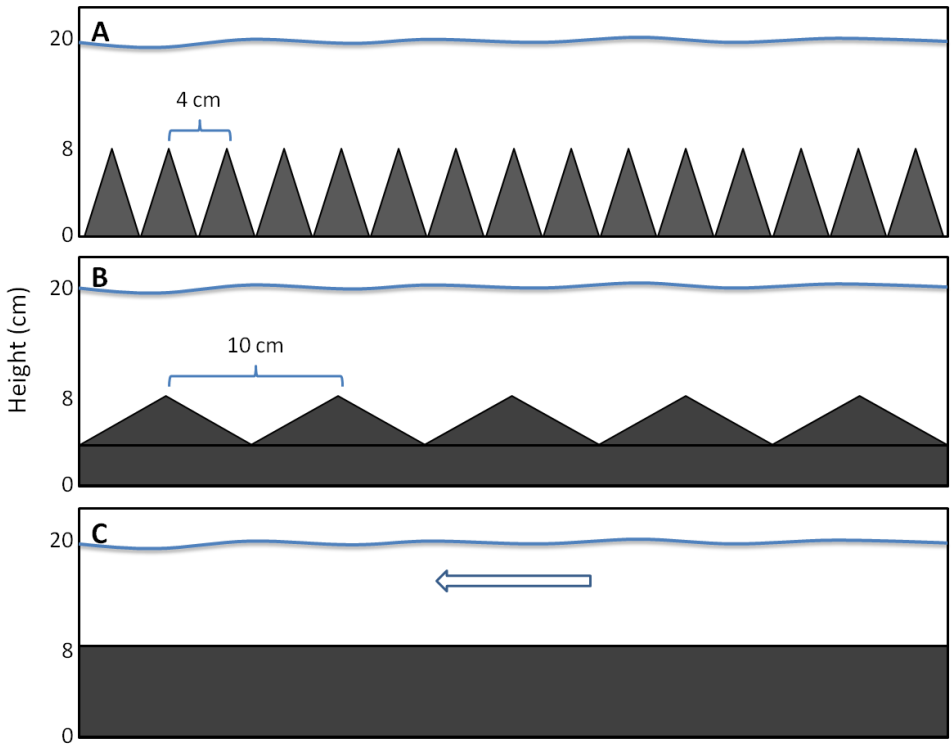

Figure 3.6: Representation of three of the structure manipulations within the test section of the flume; A) the smallest peak spacing was 4 cm; B) The greatest peak spacing considered was 10 cm and additional pieces were placed to raise the structure to the constant height; and C) as a control, video was also taken over a Plexiglas laid flat at the same height of the peaks.

Velocity and turbulence measurements were obtained using a particle image velocimetry (PIV) technique for four mean velocities, of approximately 20, 15, 10, and 5 cm/s. These velocities were first determined for each flow condition using the Marsh-

McBirney flow meter at 4/10th depth over the adjustable structure and shells and used to span the range of velocities observed *in situ* (5-30 cm s^{-1}). Velocity data was collected over multiple peak heights and spacing and were used to quantify changes in small scale hydrodynamics that could impact larval settlement. The laser was set across on supports bridging the flume walls so that the laser sheet was parallel to the walls (Figure 3.7). With the velocity, structure and laser set, the lights were turned and video was taken of the laser sheet for three minutes. Consecutive three minute videos for PIV analysis were taken using the hinged Plexiglas structures set with peak spacing of 4, 6, 8, and 10 cm.

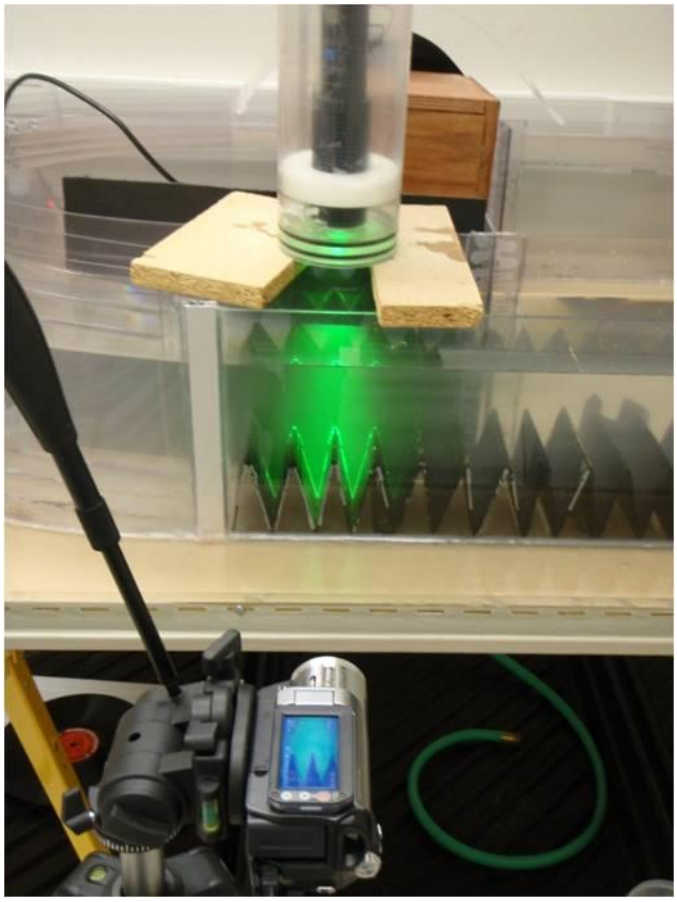

Figure 3.7: Video recorder focused on the laser sheet in the test section of the flume over structure at 4 cm peak spacing

The PIV system uses a laser and optics to create a laser light sheet that illuminates neutrally buoyant particles released into the flow (11 micron silver coated hollow glass spheres, Potter Industries©). The system consists of the camera, laser, and optics to create a 10 cm wide by 2 mm thick laser light sheet. The laser is a 30 mW 532 nm green laser diode and the beam is spread to a sheet using a 30^{o} convex glass lens. Particles are imaged using a digital video recorder. Videos were separated into 30 images per second and successive images were processed using Matlab© software that tracks particle motions over time. PIV was used to view flow in the two-dimensional plane above the structure within the flume (Figure 3.8).

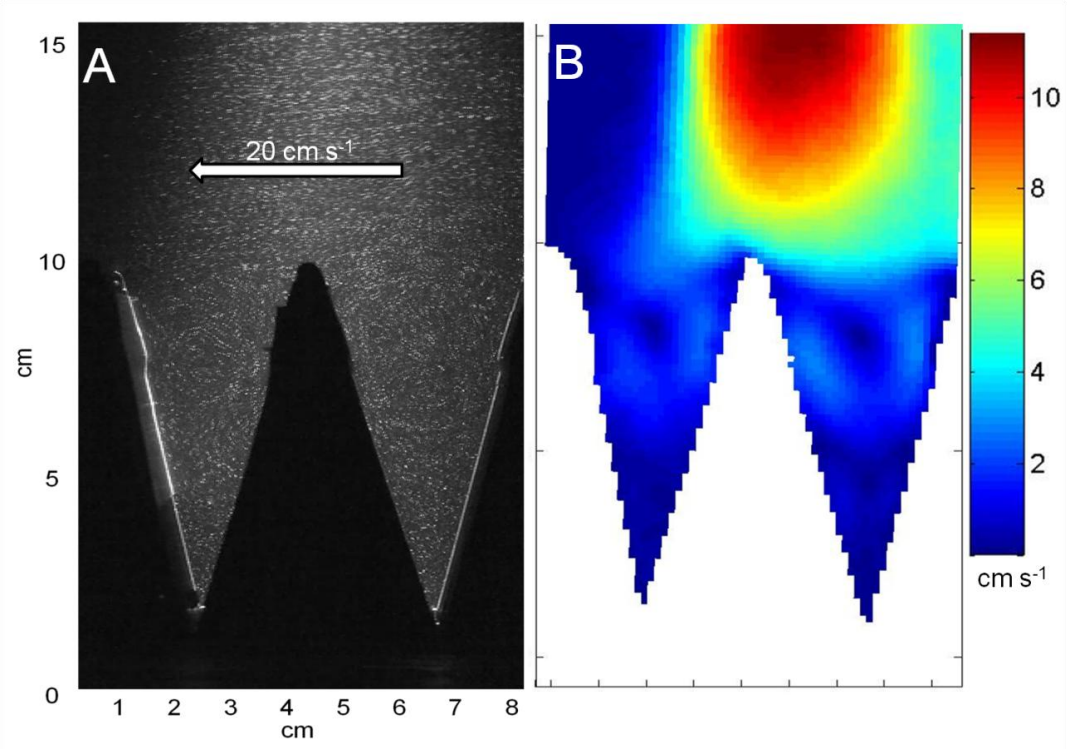

Figure 3.8: PIV images taken with 4 cm peak spacing and 20 cm $^{s-1}$ flow velocity; A) Raw image of particles illuminated by the laser; B) Instantaneous velocity (cm s^{-1}) color plot created by processing 1,000 successive images using Matlab© software that tracks particle motions over time.

The impact of the introduced structure on the mean flow conditions was determined by taking velocity measurements along vertical transects over the structure (Figure 3.9), similar to the Vectrino profiles taken over the oyster reef and restoration site in the field study.

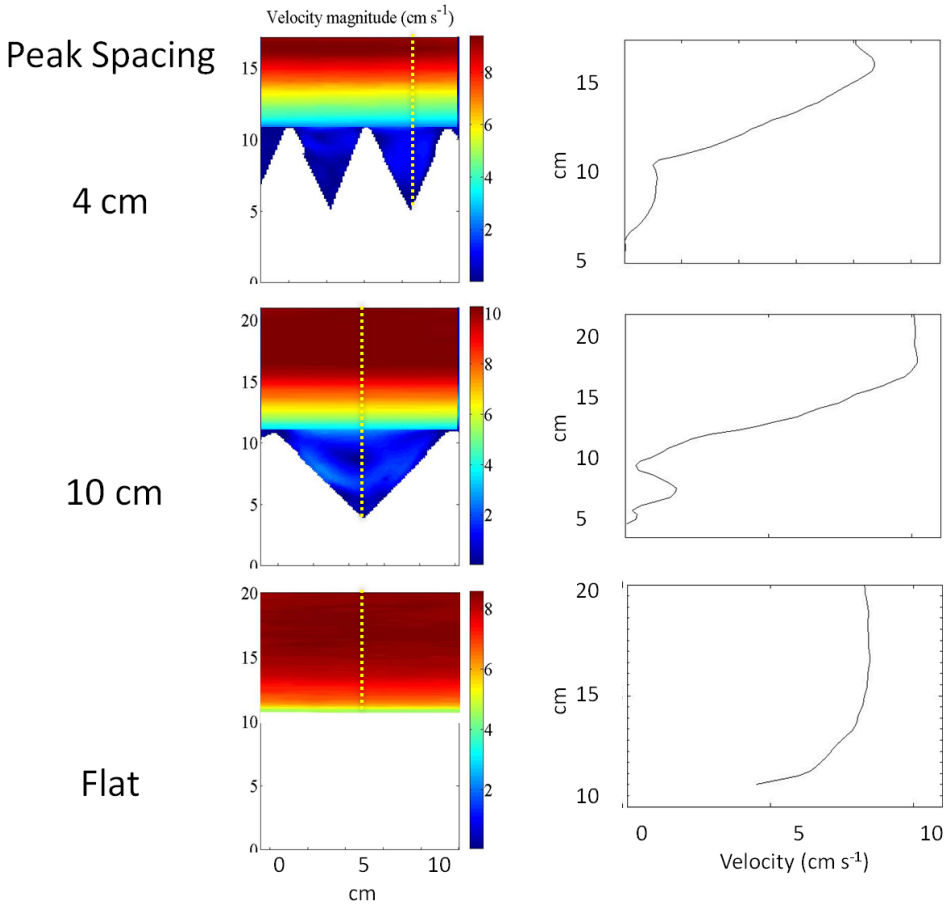

Figure 3.9: Velocity profiles were created from 50 points along a vertical transect above each structure case. Vertical transects are represented by the yellow lines in color plot of *U*. There are recirculation zones within the structure for both the 4 cm and 10 cm cases, but in the 10 cm case the velocity in the recirculation zone is greater than the velocities in the 4 cm case. Velocity increases logarithmically with height above the flat surface

Point velocities were identified along the surface of the structure to identify areas within the structure canopy where the small scale hydrodynamics such as drag and shear stress are suitable for larval settlement. This was done by taking the average of three point velocities at the surface of the structure surface at ¼, ½, and ¾ depths within the structure along the surface of the structure for each flow speed/structure manipulation. The same measurements were also done at the peak of the structure and at the deepest point within the structure.

3.3.2 Laboratory velocity profile results

Holding bulk flow velocity constant, peak spacing was increased and the velocity profiles were compared over the flat Plexiglas and for roughness with peak spacings of 4 cm and 10 cm (Figures 3.10-3.13). In all cases the flow profile over the flat Plexiglas followed the expected logorithmic profile. Within the peak structures velocities remained low (< 3 cm s^{-1}), but areas of recirculation were present in all cases. These recirculation zones, where long lived turbulent eddies are present, are represented by inversions in the velocity profiles below the depths of the peaks. One area of recirculation reaching flow speeds of 3-4 cm s^{-1} was consistently present for all 10 cm peak spacing runs and bulk flow velocities. However, two areas of recirculation were present for all 4 cm peak spacing runs at all velocities. Flow speeds reached 2-3 cm s^{-1} for the recirculation zone nearest the peaks, but the lower recirculation zones typically had flow speeds of 1 cm s^{-1} or less.

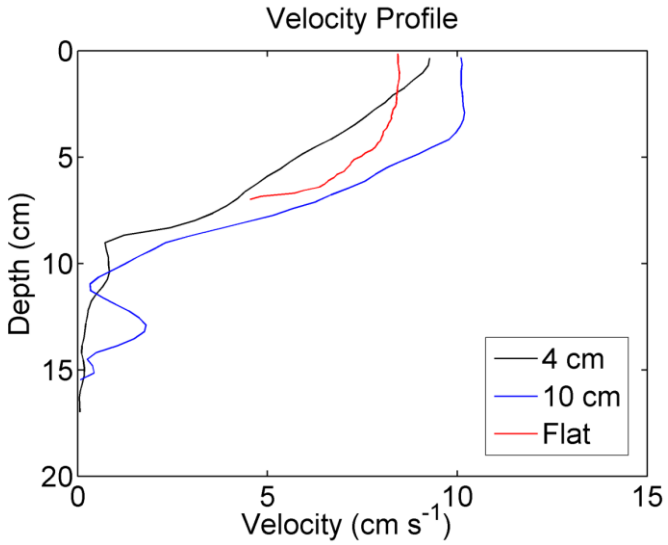

Figure 3.10: Flume velocity 5 cm s^{-1} and maximum velocity over flat Plexiglas was 8.55 cm s^{-1}

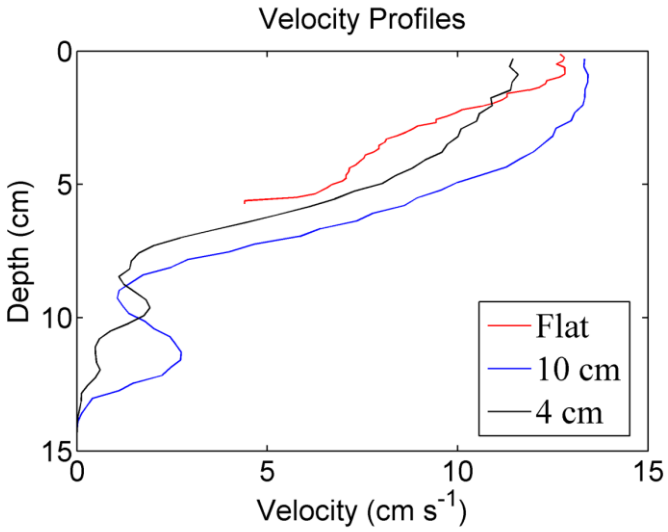

Figure 3.11: Flume velocity 10 cm s^{-1} and maximum velocity over flat Plexiglas was 13.02 cm s^{-1}

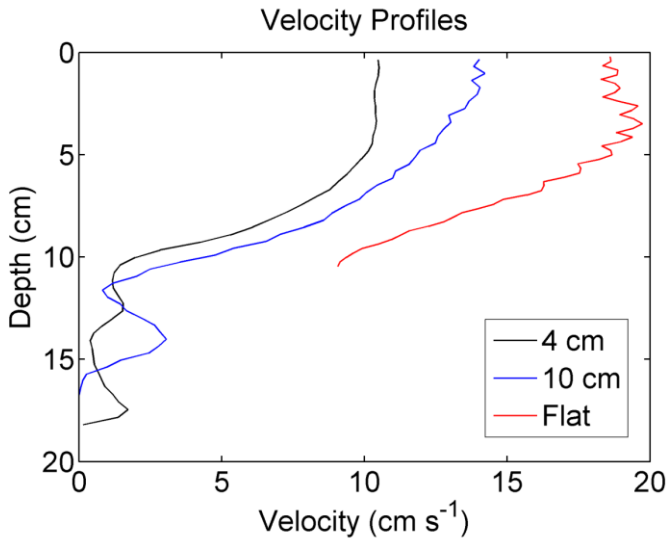

Figure 3.12: Flume velocity 14 cm s^{-1} and maximum velocity over flat Plexiglas was 20.49 cm s^{-1}

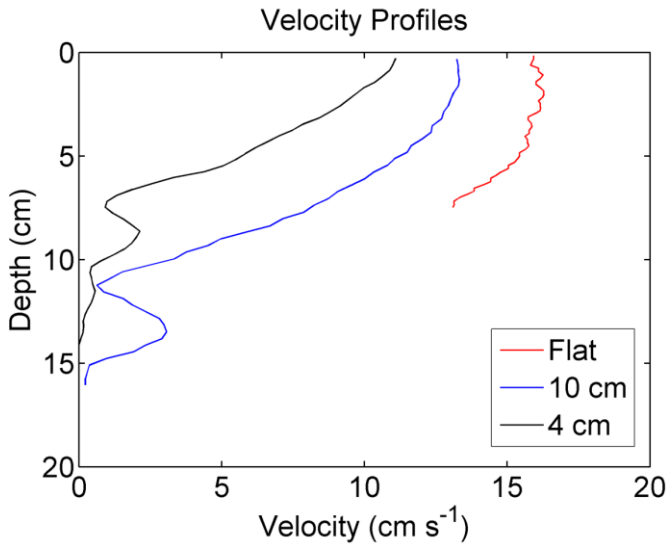

Figure 3.13: Flume velocity 20 cm s^{-1}

Velocity data became unreliable above the structure for flume velocities of 20 cm s^{-1} and 25 cm s^{-1} because the particles were moving too fast to track at 30 images per second.

3.3.3 Instantaneous drag and lift

The vector sum of the instantaneous lift, drag, and time varying acceleration reaction force (*a. r.*) are used to describe the instantaneous hydrodynamic forces acting on oyster larva, which follow the analysis described within Reidenbach *et al.* (2009). In unidirectional flow *a. r.* is minimal (Reidenbach *et al.* 2009), so the only lift and drag were needed to describe the hydrodynamic forces in this experiment.

Instantaneous drag (D) including magnitude and direction (parallel to the direction of water flow):

$$D = 0.5\rho u^2 S_p C_D \tag{3.1}$$

where ρ = 1023 kg m^{-3} is the density of seawater with salinity = 35 ppt at 25°C, u is the instantaneous velocity, $S_p = 7.07 \times 10^{-8}$ m^2 is the projected area of the 300 μm sphere (Thompson *et al.* 1996) normal to the flow direction, and $C_D = 40 / (u*d/10^{-6})$.

The instantaneous lift force (L) acts normal to the direction of water flow was calculated by:

$$L = 0.5\rho u^2 S_p C_L \tag{3.2}$$

where $S_p = 7.07 \times 10^{-8}$ m^2 is the projected area of the 300 μm sphere normal to the flow direction, and $C_L = 0.2$ (Wiberg and Smith 1985; Wiberg and Smith 1987).

Since the goal of this study was to investigate how hydrodynamics change with benthic roughness *D* and *L* were calculated for structures with spacing between roughness peaks of 4, 6, 8 and 10 cm. Velocities for calculations were averages of 40 velocity measurements spanning a ~1.5 cm distance along the surface from PIV estimates. Velocities used in the analysis were located at the mid-point of elevation between the peak and trough of the roughness element. Both *D* and *L* increase with peak spacing for all velocities used in this study (Figure 3.14 and Table 3.3). The trend is even stronger when *D* and *L* for all velocities were averaged within each peak spacing. R^2 values for *D* and *L* increased to 0.9975 and 0.9822 respectively, but the standard deviations also increase.

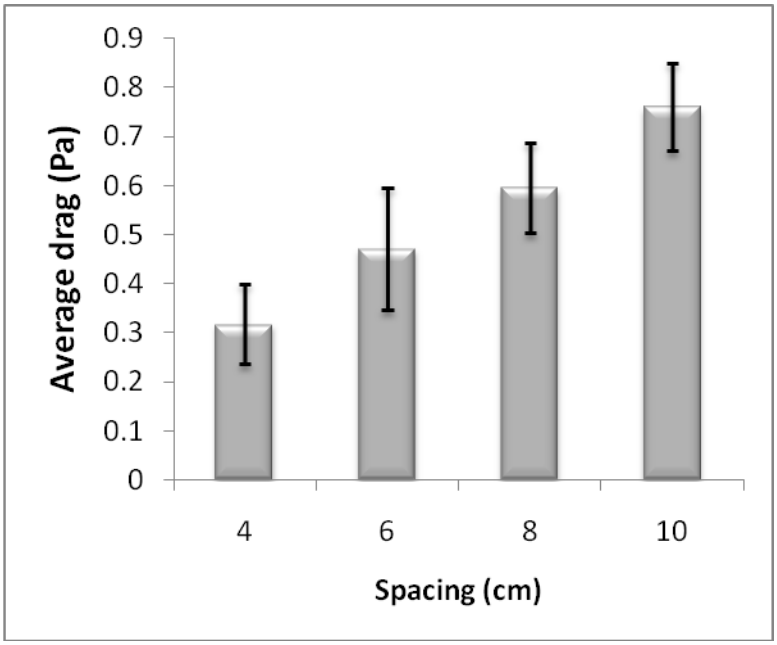

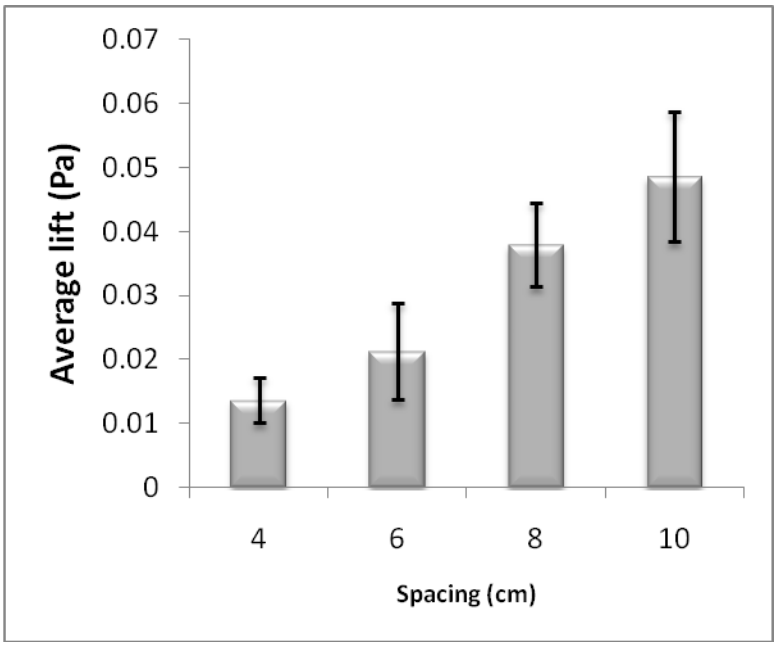

Figure 3.14: Drag and Lift in *N* +/- one standard deviation increase with peak spacing from 4 cm to 10 cm; flume velocities were averaged to illustrate trends

Among velocities *D* and *L* are significantly greater at 5 cm/s than at the three greater velocities. At the 5 cm/s mean flow condition, the turbulent eddies that formed around the peaks of the roughness elements enhanced the shear formed along the surface

at the mid-point region of the roughness, thus enhancing the lift and drag. Skimming flow occurring at higher velocities and thus D and L estimates were lower than the 5 cm/s flow condition. For flow over the flat Plexiglas, *D* and *L* increase with velocity (R^2=0.89, and R^2=0.87 respectively).

Flume Velocity (cm/s)	Drag	Lift
5	3.3E-10	1.5E-11
10	3.2E-10	1.4E-11
14	6.6E-10	6.0E-11
20	9.5E-10	1.2E-10

Table 3.2: *D* and *L* in N over flat Plexiglas

Flume Velocity (cm s^{-1})	Peak Spacing (cm)	4	6	8	10		4	6	8	10
5	Drag	1.9E-10	2.1E-10	2.9E-10	3.0E-10	Lift	1.1E-11	1.3E-11	2.6E-11	2.8E-11
	Stdev	1.3E-11	1.9E-11	1.3E-11	2.7E-11	Stdev	1.5E-12	2.4E-12	2.4E-12	5.2E-12
10	Drag	2.9E-11	7.2E-11	3.7E-11	1.0E-10	Lift	4.4E-13	1.8E-12	5.2E-13	3.3E-12
	Stdev	2.5E-11	2.5E-11	1.7E-11	2.2E-11	Stdev	8.2E-13	1.1E-12	4.3E-13	1.4E-12
14	Drag	2.9E-11	5.7E-11	1.1E-10	1.4E-10	Lift	3.2E-13	1.2E-12	4.1E-12	6.3E-12
	Stdev	1.4E-11	2.5E-11	2.4E-11	1.0E-11	Stdev	2.6E-13	9.7E-13	1.6E-12	9.0E-13
20	Drag	3.8E-11	8.4E-11	8.9E-11	1.3E-10	Lift	5.7E-13	2.7E-12	2.7E-12	5.7E-12
	Stdev	2.0E-11	4.1E-11	2.7E-11	1.9E-11	Stdev	5.5E-13	2.2E-12	1.4E-12	1.6E-12

Table 3.3: Average *D* and *L* in N of 40 point velocities, with standard deviations, for four velocities and four peak spacings

These results suggest that lower peak spacing provides refuge from hydrodynamic stresses that could wash away larvae before they are able to attach themselves to the substrate. Combined with the refuge from large predators and steep sloping sides of the

preventing burial by sediment, narrow spacing of roughness elements may provide the better habitat for recruitment than wide spacing.

3.3 Ecology in the field

3.3.1 Field structure manipulation and recruitment materials and methods

In the flume study small scale hydrodynamics over different benthic roughnesses were quantified and related to larval settlement, but other contributing factors such as sedimentation and predation were not included. To see how benthic roughness impacts larval settlement the structures used in the lab flume were replicated in a field study where sedimentation and predation occur naturally. Five replicates of three structures of varying topography were created to mimic laboratory studies using slate tile as the settlement substrate (Newell *et al.*, 2000) were set in 32 cm by 76 cm trays using Quikrete® concrete. For the first structural set the slate tiles were laid flat across the base. For the second set the tiles were cut into 30 cm by 8 cm pieces and set at angles to create an average spacing, between 11 peaks, of five cm. The tiles were also cut into 30 cm by 8 cm pieces for the third structure, but only five peaks 12 cm apart on average fit into the base. All fifteen of these structures were deployed on August 3, 2010 between HLCR2 and the restoration reefs and adjacent to the measurement site at HLCR MUD and were deployed for five months to allow oysters to settle and grow. The spawning period for *C. virginica* is June through September (Kennedy and Krantz, 1982). Figure 3.15 shows the structures on the day of deployment.

Figure 3.15: Fifteen structures deployed across HLCR MUD and between HLCR2 and HLCR 2008; HLCR2 is the reef in the background.

The narrow and wide peak spacing was used to represent different possible reef structures. During the field study portion of this thesis work comparisons between reefs of different constructions were made. HLCR2 comprised narrowly spaced, vertically growing, live oysters which provide refuge from sedimentation and predation. HLCR WHELK comprised a mound of whelk shells that create wider gaps between them because of their larger size. HLCR 2008 comprised multiple mounds of horizontally oriented fossil oyster shell which provides little refuge. When comparing the results from the structure manipulation and recruitment study to surveys done of the three different reef types, similarities are found.

After a two month period at the mud site nearly all of the structures were buried in sediment or covered in algae (Figure 3.16). The structures were then cleaned of sediment and algae and moved to higher relief areas on the hard fossil shell at HLCR 2008 so that the study could continue.

Figure 3.16: A) Initial deployment on August 3, 2010; B) Substantial sediment and algal growth observed on October 10, 2010; C) After being cleaned and moved to HLCR 2008; D) Day counts were done: January 7, 2011

3.3.2 Recruitment results

On January 7, 2011 counts of live oysters were conducted to determine recruitment success. The counts revealed that structures with narrow peak spacing had significantly more recruitment than structures with wide peak spacing (ANOVA two-factor with replication, $F_{1,16}$=33.87, p<0.05) , and a significant difference in recruitment density was found among the peaks and valleys of all structures (ANOVA two-factor with replication, $F_{1,16}$=108.27, p<0.05). The five flat tile structures were covered by sediment and showed no signs of recruitment (Figure 3.17). These results coincide with the first recirculation zones observed within the structure with 4 cm spacing in the flume

study. The wide peak spacing structure in the field also had greater recruitment on the top half, but not as much as the narrow spacing structures. The wide peak valleys had the lowest recruitment, likely due to sediment accumulation within the valleys. Possible reasons for the apparent preference of narrowly spaced roughness elements by oyster larvae likely include: larvae are brought down to the substrate by the turbulence in these zones, food is consistently delivered to settled oysters, possibly suffocating particles are unlikely to accumulate in on steep sloping surfaces where turbulence can wash them away, and protection from predation.

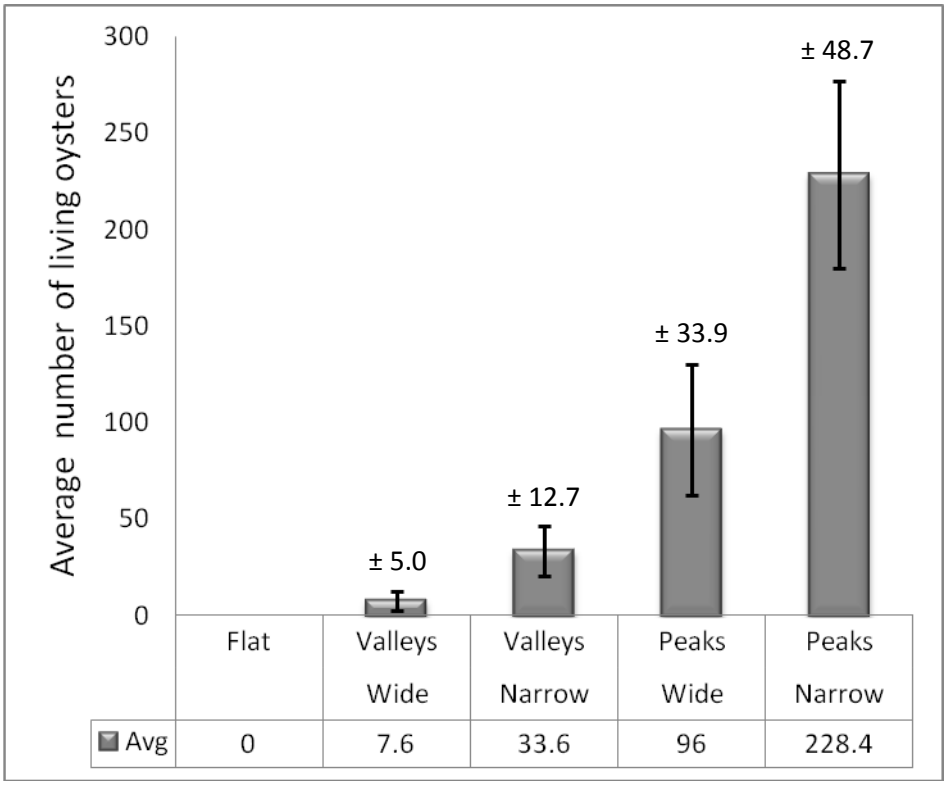

Figure 3.17: January 7, 2011 count results +/- one standard deviation for all structures; the peaks of structures with narrowly spaced peaks had the greatest recruitment and (excluding the flat tiles) the valleys of structures with widely spaced peaks had the least recruitment

Comparison of oyster size classes between structures reveals that, within five months, the majority of oysters that settled on all of the structures grew to a size of 1-2 cm (Table 3.4). Fewer smaller oysters (< 1 cm) were observed, which is consistent with a decline in settlement due to colder water temperatures discouraging spawning. The greatest difference between narrow peak spacing and wide peak spacing was found for oysters 2-3 cm in diameter. The narrow peak spacing provides refuge from predators and sedimentation which leads to lower mortality rates (Soniat *et al.*, 2006).

Size (mm)	0.1-10.0	10.1-20.0	20.1-30.0	30.1-40.0	Total
Narrow	32.0	57.0	29.0	0.0	118.0
Wide	30.0	41.0	16.0	1.0	88.0
% Narrow	27.1	48.3	24.6	0.0	100.0
% Wide	34.1	46.6	18.2	1.1	100.0

Table 3.4: Live oyster counts divided by structure (narrowly or widely spaced peaks) and size class determined by the mean diameter of each individual; percents are of the total count within each size class per structure type

TNC conducted the count of living and dead oysters in 2009 at the three different sites to monitor recruitment on the different substrates. Their results (Table 3.4) from a minimum of three sample counts using a 0.0625 m^2 quadrat also supported visual observations made during the time instruments were deployed at the sites. As roughness elements spacing increased and refuge decreases the number of oysters decreased.

Totals	HLCR2	HLCR WHELK	HLCR 2008
Live oysters	500	255	26
Dead oysters	33	16	2

Table 3.5: The Nature Conservancy survey data from 2009

2.4 Discussion of small scale hydrodynamics

In the Vectrino study small scale velocity measurements were taken along vertical transects down to within 2 cm of the substrate. Vertically oriented live oysters at HLCR2 were found to form a structure that includes reduced turbulence between individual oysters. Stresses at the healthy reef peaked at the tips of the oysters and very near to the bed at the restoration site. Along with bed roughness, TKE dissipation decreased from HLCR2 to HLCR 2008 to HLCR MUD. Momentum transport at HLCR2 is dominated by turbulent sweeps reaching into the reef, whereas at HLCR 2008 ejection and sweep events occur more equally. In a similar analysis done over a sandy benthic surface (Yuan *et al.* 2009), ejection events accounted for 56% of the turbulent sediment flux from the sandy bottom, indicating that momentum transfer is dominated by bursting events transporting turbulent motions mostly away from a low roughness bed and is responsible for sediment resuspension. The addition of roughness elements, as well as their density and geometry (Hendricks *et al.* 2006), lead to the change in direction of momentum transfer responsible for larval and food delivery to the bed.

A structure manipulation study was conducted to further investigate how benthic roughness affects small-scale hydrodynamics. For both the lab flume and field studies simplified structures of repeating vertically oriented roughness elements were constructed to mimic benthic roughness. As discussed earlier, turbulence provides transport of the

larvae to the substrate (Koehl *et al.* 2007), and food to growing oysters (Lenihan *et al.* 1996). Vertical velocity profiles compared within roughness elements below the peak of the roughness revealed two recirculation zones within the structure canopy at 4 cm spacing and only one recirculation zone at 10 cm spacing. These areas of recirculation match up closely to the areas where the greatest recruitment was observed on the slate tile structures left at the field study site for five months.

In a similar study, Soniat *et al.* (2004) looked at statistical differences in recruitment between narrowly spaced vertical shells, widely spaced vertical shells, and horizontally placed shells. Their results suggest that there is no effect of vertical structure and a negative effect of refuge on total density of oysters and on density of live oysters. However, their results also suggest that refuge and vertical structure prevent suffocation by sediment and predation and thus lead to lower oyster mortality. The results from this thesis work compliment their study by revealing that drag and lift forces both increase with roughness element spacing, but refuge area inherently decreases. Once again, supporting results come from the recruitment study, suggesting that when natural factors such as sedimentation and predation are included, narrowly spaced roughness elements provide a better oyster habitat than widely spaced roughness elements or a lack of roughness elements.

The combined field and lab results suggest that an increase in bed roughness is beneficial for larval recruitment. Narrowly spaced, vertically oriented, repeating roughness elements create an environment where momentum transfer is towards the bed,

and there are areas sheltered from intense hydrodynamics that could potentially prevent larval settlement.

Chapter 4

4.1 Discussion of major findings

The heightened focus on oyster restoration and necessity to understand the physical environment and parameters that will make restoration efforts successful were the driving forces for this field research. Due to the expansive topic, this research focused upon the role hydrodynamics plays in creating an environment conducive to larval settlement success. To review, the questions addressed in this thesis were: (1) How do elevation and bed roughness affect shear stresses and drag in the turbulent boundary layer over an intertidal oyster reefs and restoration sites; (2) How does shear stress distribution and variability differ among sites of varying topographies; and (3) How might the varying hydrodynamic conditions impact larval recruitment?

Results indicate increases in bed roughness and elevation result in conditions that support larval recruitment and oyster growth. Roughness elements provide sheltered areas where larvae have an opportunity to settle without encountering great stresses that may wash them away before they attach (Soniat *et al.* 2004, Reidenbach *et al.* 2009). TKE dissipation and momentum transfer to the bed provide transport of the larvae to the substrate (Koehl *et al.* 2007), food to growing oysters (Lenihan *et al.* 1996), flushing of food depleted water masses (Reidenbach *et al.* 2007) and resuspension of sediment (Yuan *et al.* 2009) from in-between oysters. Based on the Multi-site study, a site with vertical relief (elevation) and without roughness elements does not create the same favorable conditions for larval settlement. The mounds of fossil shell at HLCR 2008 have vertical relief similar to the historical reef. However, high hydrodynamic stresses found very near

the fossil shell bed and the lack of vertically oriented roughness elements to provide refuge from predation likely contribute to the lack of recruitment documented by TNC's 2009 survey (Table 3.4).

The combined results from this thesis work and the results from other studies included in this discussion can be applied to future restoration efforts. Elevation and benthic roughness both affect larval settlement and recruitment. Roughness elements created artificially or the addition of large roughness, such as whelk shell, to restoration sites would help to provide a turbulent environment for larval and food transport as well provide areas of refuge from predators and sedimentation. Schulte *et al.* (2009) concluded that vertical relief is necessary for successful recruitment to restoration efforts and Soniat *et al.* (2004) concluded that vertical substrate and refuge from predation are crucial to reef development.

4.2 Implications for restoration efforts

The investigation of the hydrodynamics of different reef structures, leads me to conclude that elevation, benthic roughness and refuge are all factors that should be considered in future restoration efforts.

Healthy reefs were found to have higher elevation and benthic roughness than mud or fossil shell restoration sites. On the healthy reefs higher turbulence is created above reef, but less along surfaces within reef where larvae may settle. The vertical orientation of live oysters on a healthy reef also prevents sediment from accumulating and preventing recruitment and growth.

Larvae prefer to settle on areas of high roughness but within the reef where bed shear stresses are lower. The tightly packed densities of oysters on a healthy reef may also provide protection from predation. The inclusion of whelk shell is an improvement upon current flat oyster shell restoration sites, because of its ability to increase the topographic variability of a restoration site as well as protected areas.

Improved restoration depends upon creating benthic substrates with densities and roughnesses that limit sedimentation and predation. TNC is already monitoring recruitment onto different substrates and reef structures, and they are finding greater recruitment success on sites that contain whelk shell than on those that don't. The continued use of whelk shell or the creation of beds with similar benthic topographic variability should be the focus of future restoration efforts.

Acknowledgements

This opportunity to complete my first graduate level scientific research could have been too intimidating of a task if it wasn't for the professional and personal assistance of many individuals.

First of all I would like to express my appreciation to my advisory committee: Dr. Matthew A. Reidenbach, Dr. Arthur Schwarzschild, Jerry McCormick-Ray and Dr. Karen McGlathery. Special thanks to my primary advisor Matt Reidenbach whose time, patience and understanding throughout this process were invaluable. He took the time to help me start from the beginning in a new field, allowed me to learn from my mistakes and was always available to answer my questions and concerns. The lessons I learned from Art Schwarzschild from knot tying to last minute experimental re-design will undoubtedly come in handy more often than I know. Jerry McCormick-Ray's enthusiasm for oysters and their importance was contagious, inspiring, and a continual reminder of the importance of this research. Karen McGlathery helped me take the critical step to conduct my research so that it was meaningful beyond just my study site.

My field research would not have been possible without the supportive staff of the Anheiser Busch Coastal Research Center at the Virginia Coastal Reserve LTER, my fellow graduate students and lab mates, many who offered field assistance, and The Nature Conservancy. J.C.R. (Jenny) Hansen was my partner in the field, my personal Matlab tutor, and often times emotional support and the all important comic relief. James Selph, a high school student, whom I was partnered with through the Research

Experience for High School students (REHS) program, assisted me in data collection during the summer of 2009. Thanks go to The Nature Conservancy for allowing me to conduct my research on their protected land and the supervision and assistance of Barry Truitt and Bo Lusk.

My laboratory research made possible by funding from the University of Virginia's Exploratory Research Award, Gerald Williamson's time and efforts in the machine shop constructing the recirculating flume, and Kathleen Walsh who spent many hours in the lab re-running experiments as we learned from our mistakes.

My personal experience during my time at the University of Virginia was enriched by my relationships with fellow graduate students, the Environmental Sciences faculty and staff, and my great friends. Jenny, Jenn H., Abi, Kirby, Jenn B, Katy, Neg and Rowe were there for me in countless ways over the past three years. Finally, I must acknowledge my family's support, especially my mother Linda Gardner who has paved the road that continues to lead me to great places and whose love and support is always just a phone call away.

This research was funded by a Virginia Coast Reserve Long Term Ecological Research grant by the National Science Foundation (NSF-DEB 0621014), University of Virginia, and the REHS program.

References

Arve, J. (1960). Preliminary report on attracting fish by oyster-shell plantings in Chincoteague Bay, Maryland. *Chesapeake Science, 1*(1), 58-65.

Bahr, L., & Lanier, W. (1981). The ecology of intertidal oyster reefs of the south Atlantic coast: A community profile. *US Fish and Wildlife FWS/OBS/81.15, Washington, DC, USA,*

Bartol, I. K., Mann, R., & Luckenbach, M. (1999). Growth and mortality of oysters (Crassostrea virginica) on constructed intertidal reefs: Effects of tidal height and substrate level. *Journal of Experimental Marine Biology and Ecology, 237*(2), 157-184.

Bennet, S. J., and J. L. Best (1996), Mean flow and turbulence structure over fixed ripples and
the ripple-dune transition, in Coherent Flow Structures in Open Channels, edited by P. J. Ashworth et al., pp. 281–304, John Wiley, New York.

Bergeron, N. E., & Abrahams, A. D. (1992). Estimating shear velocity and roughness length from velocity profiles. *Water Resources Research, 28*(8), 2155-2158.

Brumbaugh, R. D., Sorabella, L. A., Garcia, C. O., Goldsborough, W. J., & Wesson, J. A. (2000). Making a case for community-based oyster restoration: An example from hampton roads, Virginia, U. S. A. *Journal of Shellfish Research, 19*(1), 467-472.

Bushek, D. (1988). Settlement as a major determinant of intertidal oyster and barnacle distributions along a horizontal gradient. *Journal of Experimental Marine Biology and Ecology, 122*(1), 1-18.

Carriker, M., Gaffney, P., Kennedy, V., Newell, R., & Eble, A. (1996). The eastern oyster: Crassostrea virginica. *Kennedy VS, Newell RIE, Eble AF A Catalogue of Selected Species of Living Oysters of the World.Maryland Sea Grant College Program, College Park,*

Cerco, C. F., & Noel, M. R. (2007). Can oyster restoration reverse cultural eutrophication in Chesapeake Bay? *Estuaries and Coasts, 30*(2), 331-343.

Cheng, R. T., Ling, C. H., Gartner, J. W., & Wang, P. (1999). Estimates of bottom roughness length and bottom shear stress in South San Francisco Bay, California. *Journal of Geophysical Research, 104*(C4), 7715-7728.

Coen, L. D., & Luckenbach, M. W. (2000). Developing success criteria and goals for evaluating oyster reef restoration: Ecological function or resource exploitation? *Ecological Engineering, 15*(3-4), 323-343.

Crimaldi, J. P., Thompson, J. K., Rosman, J. H., Lowe, R. J., & Koseff, J. R. (2002). Hydrodynamics of larval settlement: The influence of turbulent stress events at potential recruitment sites. *Limnology and Oceanography, 47*(4), 1137-1151.

Dame, R. F., Zingmark, R. G., & Haskin, E. (1984). Oyster reefs as processors of estuarine materials*. *Journal of Experimental Marine Biology and Ecology, 83*(3), 239-247.

Dennison, W. C., & Alberte, R. S. (1985). Role of daily light period in the depth distribution of Zostera marina(eelgrass). *Marine Ecology Progress Series.Oldendorf, 25*(1), 51-61.

Eckman, J., Savidge, W., & Gross, T. (1990). Relationship between duration of cyprid attachment and drag forces associated with detachment of Balanus amphitrite cyprids. *Marine Biology, 107*(1), 111-118.

Fréchette, M., Butman, C. A., & Geyer, W. R. (1989). The importance of boundary-layer flows in supplying phytoplankton to the benthic suspension feeder, Mytilus edulis L. *Limnology and Oceanography, 34*(1), 19-36.

Fuchs, H. L., Neubert, M. G., & Mullineaux, L. S. (2007). Effects of turbulence-mediated larval behavior on larval supply and settlement in tidal currents. *Limnology and Oceanography, 52*(3), 1156-1165.

Galtsoff, P. S. (1964). The american oyster crassostrea virginica gmelin. *Fishery Bulletin*

Grass, A. (1971). Structural features of turbulent flow over smooth and rough boundaries. *Journal of Fluid Mechanics, 50*(02), 233-255.

Gross, T. F., & Nowell, A. R. M. (1983). *Continental Shelf Research, 2*(2-3), 109-126.

Hadfield, M. (2007). Individual-based model of larval transport to coral reefs in turbulent, wave-driven flow: Behavioral responses to dissolved settlement inducer. *Mar Ecol Prog Ser, 335*, 1-18.

Harwell, M. C., & Orth, R. J. (1999). Eelgrass (Zostera marina L.) seed protection for field experiments and implications for large-scale restoration. *Aquatic Botany, 64*(1), 51-61.

Haven, D. S., & Morales-Alamo, R. (1966). Aspects of biodeposition by oysters and other invertebrate filter feeders. *Limnology and Oceanography, 11*(4), 487-498.

Hendriks, I. E., Van Duren, L. A., & Herman, P. M. J. (2006). Turbulence levels in a flume compared to the field: Implications for larval settlement studies. *Journal of Sea Research, 55*(1), 15-29.

Jonsson, P., van Duren, L., Amielh, M., & Asmus, R. Making water flow: A comparison of the hydrodynamic characteristics of 12 different benthic biological flumes. *Aquat.Ecol, 40*, 409–438.

Kemp, W., Boynton, W., Adolf, J., Boesch, D., Boicourt, W., Brush, G., et al. (2005). Eutrophication of Chesapeake Bay: Historical trends and ecological interactions. *Marine Ecology Progress Series, 303*, 1-29.

Kennedy, V., & Krantz, L. (1982). Comparative gametogenic and spawning patterns of the oyster Crassostrea virginica (gmelin) in central Chesapeake Bay. *J.Shellfish Res, 2*(2), 133-140.

Koehl, M., & Hadfield, M. (2004). Soluble settlement cue in slowly moving water within coral reefs induces larval adhesion to surfaces. *Journal of Marine Systems, 49*(1-4), 75-88.

Koehl, M. (2007). Mini review: Hydrodynamics of larval settlement into fouling communities. *Biofouling, 23*(5), 357-368.

Koehl, M.A.R. and M. Hadfield. (2010) Hydrodynamics of larval settlement from a larva's point of view. Integr. Comp. Biol. 50 : 539-551.

Krause-Jensen, D., Sagert, S., Schubert, H., & Boström, C. (2008). Empirical relationships linking distribution and abundance of marine vegetation to eutrophication. *Ecological Indicators, 8*(5), 515-529.

Lacey, R. W. J., & Roy, A. G. (2008). Fine-scale characterization of the turbulent shear layer of an instream pebble cluster. *Journal of Hydraulic Engineering, 134*, 925.

Lenihan, H. S., & Peterson, C. H. (1998). How habitat degradation through fishery disturbance enhances impacts of hypoxia on oyster reefs. *Ecological Applications, 8*(1), 128-140.

Lenihan, H. S., Peterson, C. H., & Allen, J. M. (1996). Does flow speed also have a direct effect on growth of active suspension-feeders: An experimental test on oysters. *Limnology and Oceanography, 41*(6), 1359-1366.

Lenihan, H. S. (1999). Physical–biological coupling on oyster reefs: how habitat structure influences individual performance. *Ecological Monographs, 69*(3), 251-275.

Loosanoff, V. L. (1965). Gonad development and discharge of spawn in oysters of long island sound. *Biological Bulletin, 129*(3), 546-561.

Lu, S., & Willmarth, W. (1973). Measurements of the structure of the Reynolds stress in a turbulent boundary layer. *Journal of Fluid Mechanics, 60*(03), 481-511.

McCormick-Ray, M. G. (1998). Oyster reefs in 1878 seascape pattern—Winslow revisited. *Estuaries and Coasts, 21*(4), 784-800.

MacKenzie, C. (1983). To increase oyster production in the northeastern united states. *Marine Fisheries Review, 45*(3), 1-22.

McGlathery, K. J. (2001). Macroalgal blooms contribute to the decline of seagrass in nutrient-enriched coastal waters. *Journal of Phycology, 37*(4), 453-456.

Michael Kemp, W., Batleson, R., Bergstrom, P., Carter, V., Gallegos, C. L., Hunley, W., et al. (2004). Habitat requirements for submerged aquatic vegetation in Chesapeake Bay: Water quality, light regime, and physical-chemical factors. *Estuaries and Coasts, 27*(3), 363-377.

Nelson, K. A., Leonard, L. A., Posey, M. H., Alphin, T. D., & Mallin, M. A. (2004). Using transplanted oyster (Crassostrea virginica) beds to improve water quality in small tidal creeks: A pilot study. *Journal of Experimental Marine Biology and Ecology, 298*(2), 347-368.

Newell, R. I. E., Kemp, W. M., Hagy, J., Cerco, C. F., Testa, J. M., & Boynton, W. R. (2007). Top-down control of phytoplankton by oysters in Chesapeake Bay, USA: Comment on Pomeroy et al.(2006). *MARINE ECOLOGY-PROGRESS SERIES-, 341*, 293.

Newell, R. (1988). Ecological changes in Chesapeake Bay: Are they the result of overharvesting the American oyster, Crassostrea virginica. *Understanding the Estuary: Advances in Chesapeake Bay Research, 129*, 536–546.

Newell, R., Alspach, G., Kennedy, V., & Jacobs, D. (2000). Mortality of newly metamorphosed eastern oysters (Crassostrea virginica) in mesohaline Chesapeake Bay. *Marine Biology, 136*(4), 665-676.

Orth, R. J., Luckenbach, M. L., Marion, S. R., Moore, K. A., & Wilcox, D. J. (2006). Seagrass recovery in the delmarva coastal bays, USA. *Aquatic Botany, 84*(1), 26-36.

Pomeroy, L. R., D Elia, C. F., & Schaffner, L. C. (2007). Top-down control of phytoplankton by oysters in chesapeake Bay, USA: Reply to newell et al.(2007). *Marine Ecology Progress Series, 341*, 299-301.

Pomeroy, L. R., D'Elia, C. F., & Schaffner, L. C. (2006). Limits to top-down control of phytoplankton by oysters in Chesapeake Bay. *Marine Ecology Progress Series, 325*, 301-309.

Reidenbach, M. A., Koseff, J. R., & Koehl, M. (2009). Hydrodynamic forces on larvae affect their settlement on coral reefs in turbulent, wave-driven flow. *Limnol.Oceanogr, 54*(1), 318-330.

Reidenbach, M. A., Koseff, J. R., & Monismith, S. G. (2007). Laboratory experiments of fine-scale mixing and mass transport within a coral canopy. *Physics of Fluids, 19*, 075107.

Rothschild, B., Ault, J., Goulletquer, P., & Heral, M. (1994). Decline of the Chesapeake Bay oyster population: A century of habitat destruction and overfishing. *Marine Ecology Progress Series.Oldendorf, 111*(1), 29-39.

Schulte, D. M., Burke, R. P., & Lipcius, R. N. (2009). Unprecedented restoration of a native oyster metapopulation. *Science, 325*(5944), 1124.

Thompson, R. J., R.I.E. Newell, V.S. Kennedy, and R. Mann. 1996. Reproduction and Larval Development. Pages 335-370, Chapter 9 In: V.S. Kennedy, R.I.E. Newell and A. Eble (eds.). The Eastern Oyster, Crassostrea virginica. Maryland Sea Grant Publication.

Wethey, D. S. (1986). Ranking of settlement cues by barnacle larvae: Influence of surface contour. *Bulletin of Marine Science, 39*(2), 393-400.

Wiberg, P. L., & Smith, J. D. (1985). A theoretical model for saltating grains in water. *Journal of Geophysical Research, 90*(C4), 7341-7354.

Wiberg, P. L., & Smith, J. D. (1987). Calculations of the critical shear stress for motion of uniform and heterogeneous sediments. *Water Resources Research, 23*(8), 1471-1480.

Wildish, D., & Kristmanson, D. (1979). Tidal energy and sublittoral macrobenthic animals in estuaries. *Journal of the Fisheries Research Board of Canada, 36*(10)

Yuan, Y., Wei, H., Zhao, L., & Cao, Y. (2009). Implications of intermittent turbulent bursts for sediment resuspension in a coastal bottom boundary layer: A field study in the western yellow sea, china. *Marine Geology, 263*(1-4), 87-96.

Zimmerman, R., Minello, T., Baumer, T., & Castiglione, M. (1989). Oyster reef as habitat for estuarine macrofauna. *National Oceanic and Atmospheric Administration Technical Memorandum NMFS-SEFC-249*

Appendix I

Suspended sediment

To determine suspended sediment concentrations optical backscatter recorders (OBS, Campbell Scientific OBS3+©), sampling simultaneously used to collect suspended particle data. OBS recorders are connected to ADVs and AQDPs whenever they are deployed. The data is recorded using the internal memory of the ADVs and AQDPs. Since the measurement volume for the OBSs are unknown the deployment technique was changed from upward facing for all deployments in 2009 to downward facing for all deployments in 2010. When deployed with ADVs the OBSs were always deployed facing downward from the aluminum frame.

The analysis of the OBS sediment data is dependent upon ambient sediment properties, so correlation curves were empirically derived for each OBS. Sediment was collected from HLCR 2008, HLCR WHELK, HLCR MUD, and on either side of HLCR2. The pairing of OBS' and instruments was kept constant among experiments so that correlation curves were created using the instrument (AQDP or ADV) and OBS. Three 10 ml subsamples of water were collected, filtered, dried, and weighed to get the average background starting concentration. Enough water was added to the collected sediment to turn it into very wet mud. Again, three 10 ml subsamples of this were collected and analyzed in the same manner as the water. For each combination the instrument and OBS were placed in a clean (i.e., no added sediment) salt water for approximately 30 seconds. 1 TBS (14.79 ml) of the well-mixed corresponding mud

mixture was then added and well mixed with into the container of water and a measurement was taken from the OBS. With the instruments taken completely out of the water in between, 1 TBS of mud slurry was added at a time for up to 2.5 cups (591 ml). The 30 second data recordings from the OBS were averaged to come up with one data point for each known sediment concentration. A best fit line was fit to all of the data points for each of the instrument combinations to create correlation curves (Figure A.I.1).

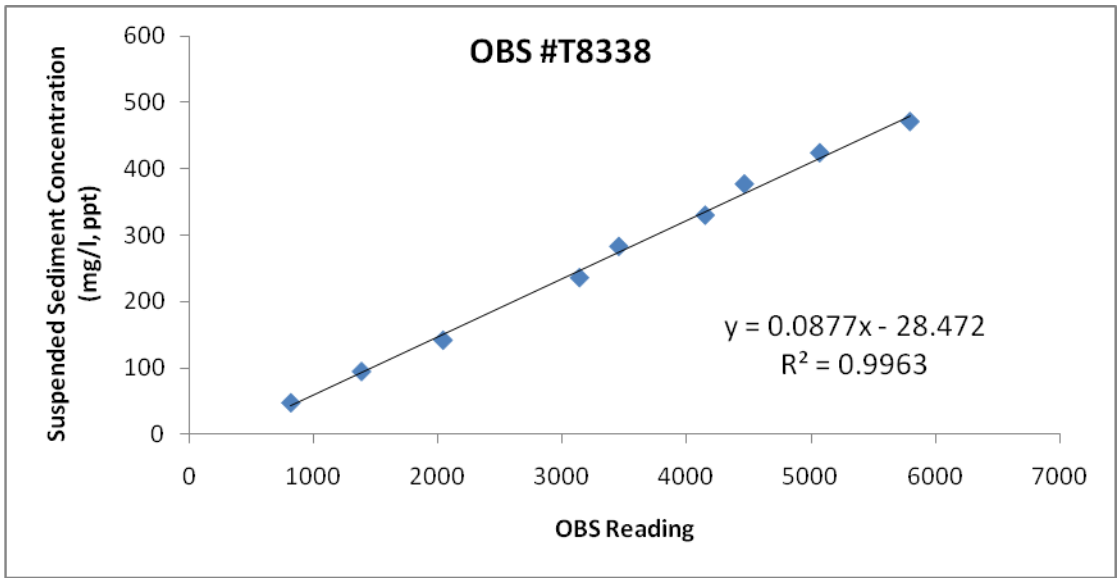

Figure A.I.1: Sample correlation curve for OBS #T8338 and paired AQDV; All curves had an R^2 value greater than 0.99, so there is a high level of confidence in the calibration.

Sediment dynamics and filtration by the oyster community

In the first of several large scale flow experiments, bulk flow across the reef was measured and the net effect of the reef on suspended sediment was quantified. The instrumentation used in this study collected data regarding how the vertical relief of the historical reef, HLCR2, influences water column turbulence and mean flow rates and how

the filtering capacity of the oysters affects suspended sediment levels and sedimentation. Figure A.I.2 depicts the instrumentation of the reef for the sediment filtration experiment. Large scale flow patterns across the reef were measured by placing ADVs at locations on either side of the reef and an AQDP on top of the reef, along a horizontal transect, aligned as best as possible with the dominant flow direction.

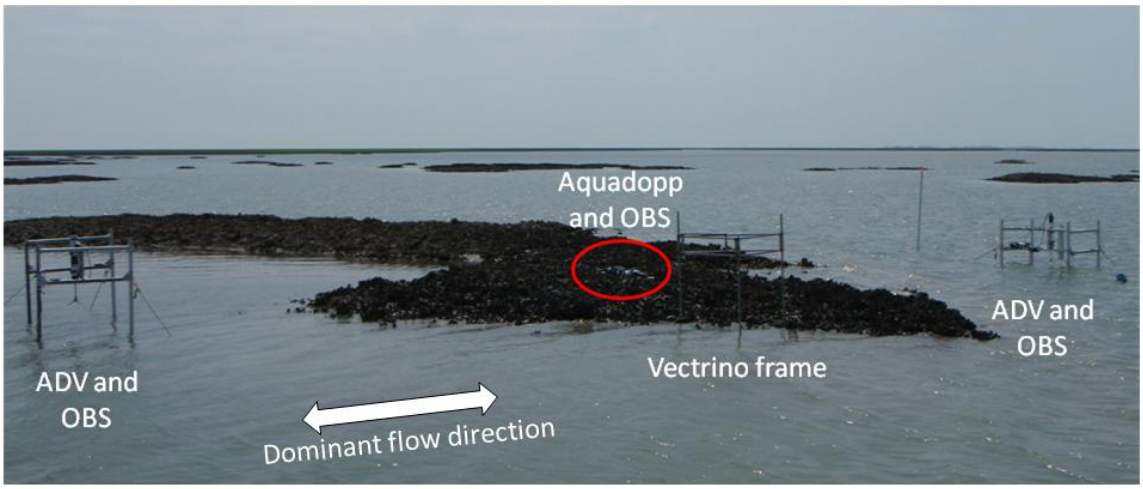

Figure A.I.2: Instruments aligned with the dominant flow to study how the vertical relief of the reef influences bulk flow, and to determine the effects of filtration on sediment uptake by the reef

Velocity data from the two ADVs was plotted together with time to identify differences between the flow upstream and downstream of the reef. Differences between the two during ebb, flood, and slack tides were focused on to identify any patterns. To determine the affects of the reef on suspended sediment concentrations three optical backscatter recorders (OBS), sampling simultaneously, were collected suspended particle data. These OBS sensors were connected to and data was recorded by each of the two ADVs flanking the oyster reef and the AQDP located at the center of the reef. Sediment uptake by the filtering of the reef was approximated using differencing of the upstream

and downstream sediment measurements along the dominant flow path. A negative difference between the downstream and upstream OBS' indicates a net uptake of sediment by the oysters, whereas a positive difference indicates a net resuspension by the bed. Figure A.I.3-D shows the concentration gradient between the east and west sides of the oyster reef.

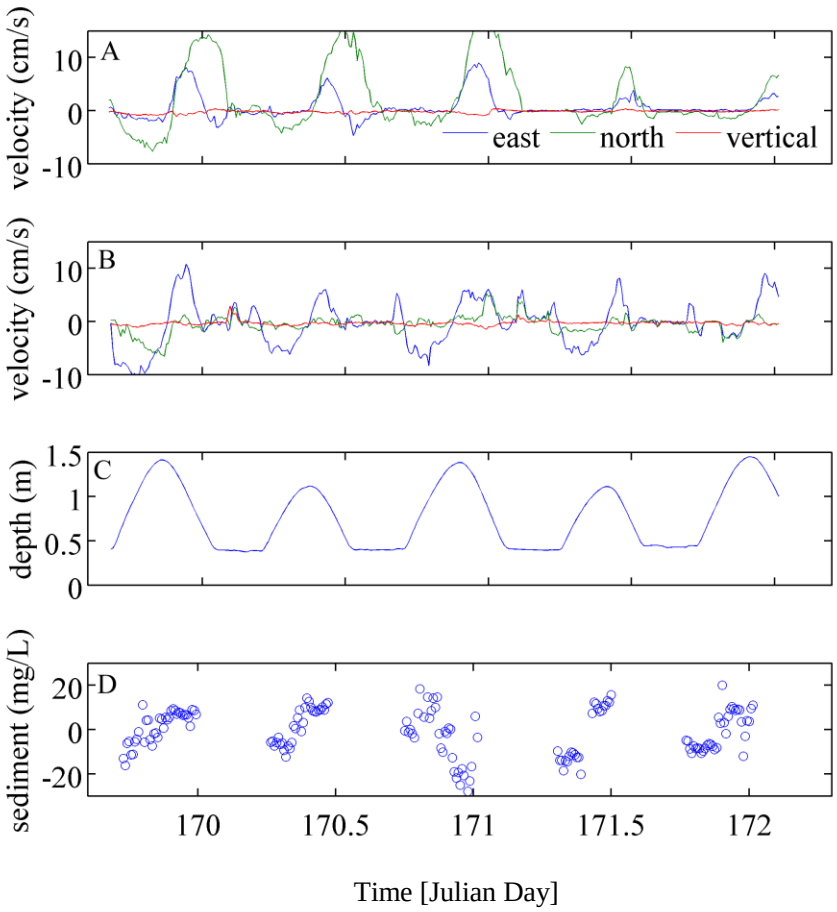

Figure A.I.3: (A) Velocities west of oyster reef. (B) Velocities east of oyster reef. (C) Water depth above reef. (D) Suspended sediment concentration gradient between the west and east side of the oyster reef.

Figure A.I.4 shows that net uptake of sediment by the reef community increased with increasing mean velocity. Greater flow speeds lead to greater vertical mixing that provides a constant supply of water containing food, and prevents a layer of seston depleted water at the reef's surface (Wildish and Kristmanson 1979, Frechette *et al.* 1989, Lenihan *et al.* 1996). The feeding oysters under these conditions have access to more of the water column, and have the opportunity to filter more suspended sediment along with their food.

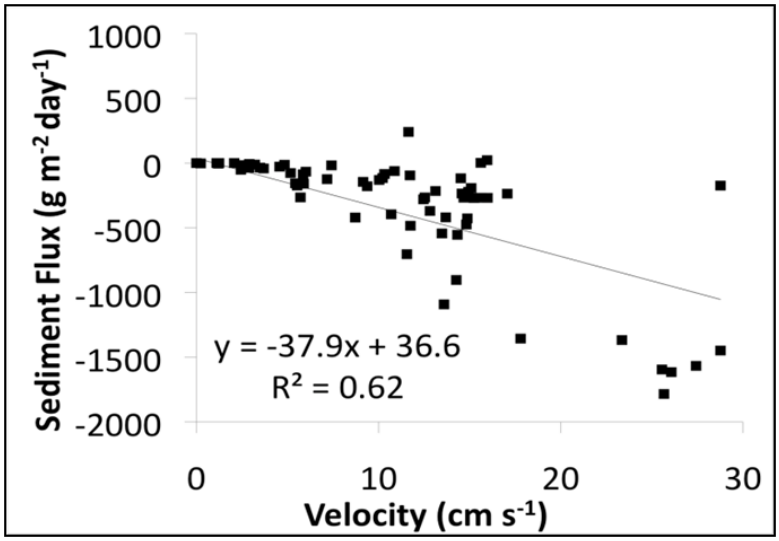

Figure A.I.4: Sediment uptake as a function of mean velocity across the oyster reef; Uptake rate was calculated using the difference between upstream and downstream sediment concentrations.

In the suspended solids study, SSC was recorded both upstream and downstream of HLCR2. The effect of the oyster community at HLCR2 on SSC appeared to be depletion of SSC as the water flowed over the reef. This may be a result of active filtration by the feeding oysters that, on a small scale, has been documented in other studies (e.g. Nelson *et al.*, 2004; Porter *et al.*, 2004; Cerco and Noel, 2007). However, if

the depletion of suspended solids by one oyster reef could be scaled up to a bay size area the benefits to oyster reef restoration could be substantial (Newell 1988, Newell *et al.* 2007). Pomeroy *et al.*, (2006 and 2007) disputes the theory that oyster restoration to historical masses would be capable of directly controlling phytoplankton blooms, but the affects of oyster filtration observed in this study would likely impact adjacent ecosystems such as seagrass meadows and species that depend on them. Aquatic vegetation including *Zostera marina*, the seagrass species that is the focus of a massive restoration effort in the coastal bays of the Delmarva Peninsula (Harwell and Orth 1999, Orth *et al* 2006), has a minimum light requirement for growth and survival (Kemp *et al.* 2004). The depletion of suspended solids and nutrients, provided by adjacent oyster reefs, would allow light to penetrate deeper into the water column which would increase the depth distribution and density of seagrass (Dennison and Alberte 1985, Krause-Jensen *et al.* 2000, McGlathery 2001) would create a positive feedback for seagrass growth. However, given current oyster populations it is unlikely that they exert a strong control on bulk SSC concentrations within the coastal bays.

Appendix II

AQDP plots

Dominant flow was consistently observed coming from the channel, across the site in a Northeast/Southwest direction. When the water is still relatively deep, a strong southerly current is present. At all sights velocities drop to 0 cm/s during slack tide.

Elevation

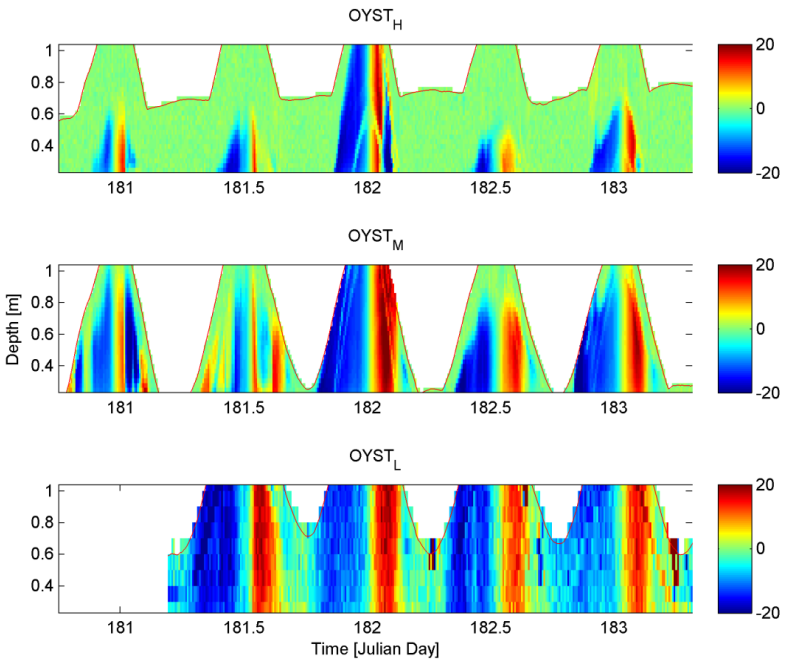

Figure A.II.1: East velocities over 5 consecutive tidal cycles taken simultaneously at 3 elevations

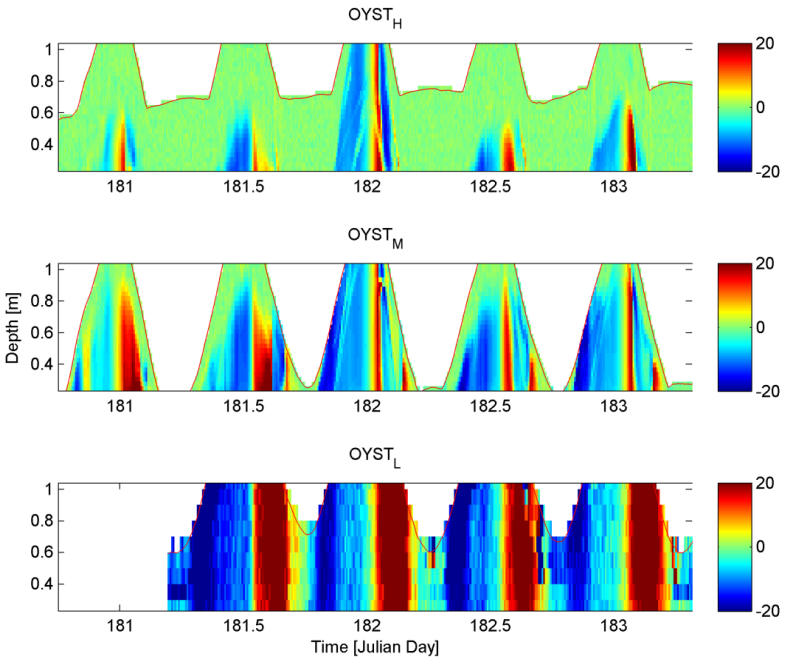

Figure A.II.1: North velocities over 5 consecutive tidal cycles taken simultaneously at 3 elevations

Various bed substrates: Multi-site study

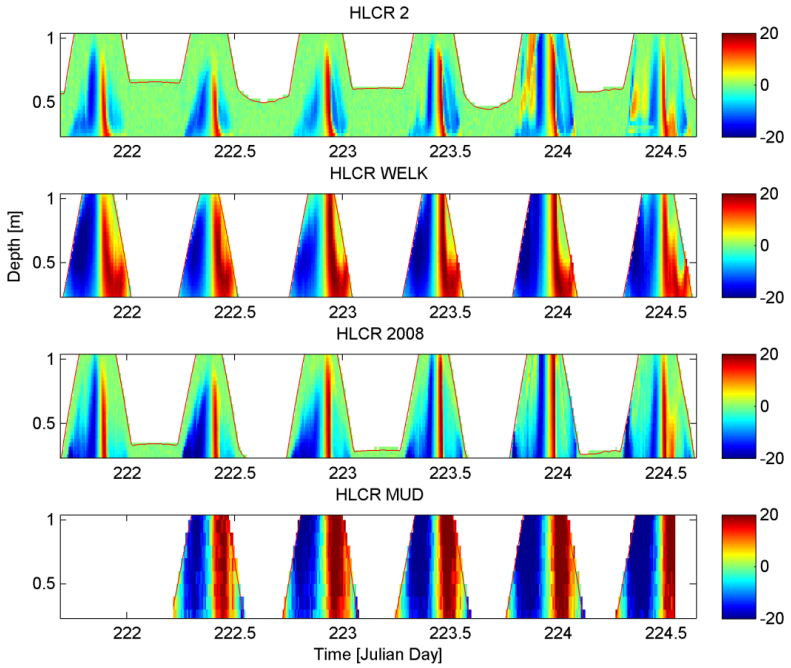

Figure A.II.3: East velocities over five consecutive tidal cycles taken simultaneously at the four sites

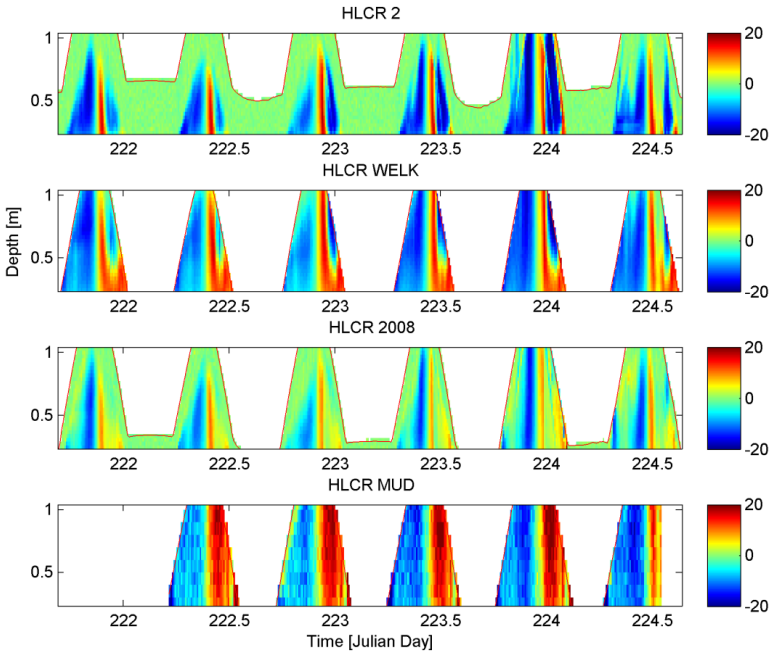

Figure A.II.4: North velocities over five consecutive tidal cycles taken simultaneously at the four sites